Total-energy and band-structure calculations for the semimagnetic $Cd_{1-x}Mn_xTe$ semiconductor alloy and its binary constituents

Su-Huai Wei and Alex Zunger
Solar Energy Research Institute, Golden, Colorado 80401
(Received 24 June 1986)

Spin-polarized, self-consistent local-spin density total-energy and band-structure calculations have been performed for CdTe, antiferromagnetic (AF) MnTe in its NiAs structure, ferromagnetic (F) $CdMnTe_2$, and the hypothetical zinc-blende phase of MnTe in the F and AF spin arrangements. We find the following: (i) The alloy environment stabilizes a zinc-blende form of MnTe, hitherto unknown to exist in the phase diagram of pure MnTe. Its calculated Mn—Te bond length (2.70 ± 0.02 Å) is very close to that observed in the alloy (2.73 Å), but is substantially different from the Mn—Te bond length in pure (NiAs-type) MnTe (2.92 Å). (ii) AF zinc-blende MnTe is more stable than F zinc-blende MnTe due to a reduced p-d repulsion in the upper valence states. (iii) F $Cd_{1-x}Mn_xTe$ is more stable than its zinc-blende constituents CdTe + F MnTe, hence, once formed, this ordered alloy will not disproportionate. (iv) Nevertheless, AF $CdMnTe_2$ is more stable than its ferromagnetic counterpart, but it is unstable relative to its constituents CdTe + AF MnTe. Hence, if F $CdMnTe_2$ converts into AF $CdMnTe_2$, the latter will disproportionate into antiferromagnetic domains of MnTe. (v) The band structure of F zinc-blende MnTe and F $CdMnTe_2$ predicts a novel type of negative (p-d) exchange splitting, whose origins are discussed in terms of a p-d repulsion mechanism. (vi) The calculated electronic states of $Cd_{1-x}Mn_xTe$ show a vanishing optical bowing, a Mn $d_\uparrow$ band at $E_v-2.5$ eV and explains the observed optical transitions. (vii) The fact that $Cd_{1-x}Mn_xTe$ does exhibit localized multiplet transitions but NiAs-type MnTe does not, is explained in terms of the coexistence of covalency and low symmetry in the latter case. We discuss the electronic structures, local magnetic moments, exchange interaction coefficients, and the general features of the chemical bonds in the semimagnetic semiconductor.

I. INTRODUCTION

Manganese doped II-VI compounds $A^{II}_{1-x}Mn_xC^{VI}$ have recently attracted considerable attention[1,2] as they exhibit the interesting combinations of magnetism[3–5] and semiconductivity,[6] impuritylike localization phenomena[7–9] and itinerant, bandlike characteristics,[6,10] as well as spin-glass behavior[3] and antiferromagnetism.[3] These systems are distinct from conventional octet isovalent semiconductor alloys[11] (e.g., III-V alloys such as $A^{III}_{1-x}B^{III}_xC^{V}$, or II-VI alloys such as $A^{II}_{1-x}B^{II}_xC^{VI}$) in that they include an open-shell Mn d^5 ion, and differ from dilute d-electron impurity systems[12] (e.g., $3d$ impurities in III-V or II-VI semiconductors) in that MnC^{VI} compounds show considerable solid solubility in common-anion $A^{II}C^{VI}$ compounds despite large lattice mismatches and different crystal structures. The $A^{II}_{1-x}Mn_xC^{VI}$ system hence provides a unique link between impurity and alloy physics in semiconductors systems.

$Cd_{1-x}Mn_xTe$ is probably the most extensively studied member of the $A^{II}_{1-x}Mn_xC^{VI}$ group. It crystallizes in a single-phase zinc-blende (ZB) structure up to a composition[13] of $x=0.7$. Above this composition, multiphase structures prevail. In this alloy the cadmium atoms, located on a face-centered cubic (fcc) sublattice, are substituted by manganese atoms. Low-field magnetic susceptibility and specific-heat measurements by Galazka, Nagata, and Keesom[3] suggested three ranges of composition with different magnetic properties: (i) For $x\leq0.17$, the alloy is paramagnetic; (ii) for $0.17<x\leq0.60$, a spin-glass phase is observed; and (iii) for $0.60<x\leq0.70$ the antiferromagnetically ordered phase has been suggested. Antiferromagnetic (AF) exchange interactions are thought to be responsible for these magnetic phase transitions.[3] The exchange constant J_{dd} has been measured[14,15] and found to be antiferromagnetic (i.e., attractive for unlike spins) both for nearest and for next-nearest neighbors. A theoretical study[16] using a generalized Anderson Hamiltonian found superexchange interaction to be dominant at nearest- and next-nearest-neighbor sites. Spin-spin exchange interaction constants $N_0\alpha$ and $N_0\beta$, between the localized moment of the Mn $3d^5$ electrons and the band electrons have also received considerable attention.[5,17,18] It is because of this interaction that magneto-optical properties of semimagnetic semiconductors are qualitatively different from those observed in their nonmagnetic counterparts. $N_0\alpha$ and $N_0\beta$ have been obtained by simultaneous measurements of magnetoreflectivity and magnetic moment on $Cd_{1-x}Mn_xTe$.[5] A recent theoretical study[17] estimated these quantities using the band-structure calculation within the local-spin-density formalism. The observed abnormally large negative value of $N_0\beta$ has been explained using a resonant scattering model.[18]

While experimental studies of bulk $Cd_{1-x}Mn_xTe$ have been extensive, some fundamental problems still remain, such as whether the Mn ions are randomly distributed in the crystal, the location of the energy levels of the Mn $3d$ states, the magnitude of Mn $3d$ and Te $5p$ hybridization

and the nature of the low-energy electronic transitions. Reported results regarding the Mn $3d$ energy levels are rather controversial. Photoemission measurement of $Cd_{1-x}Mn_xTe$ by Webb *et al.*[19] found the Mn $3d$ states 3.5 eV below the valence band (v) maximum E_v, whereas similar experiment by Orlowski[20] place the same states at E_v-6 eV and photoluminescence measurement by Vecchi *et al.*[21] infer these states at $E_v-0.8$ eV. Although it is commonly assumed in coordination chemistry of divalent manganese that the Mn $3d^5$ states are highly localized in the $^6A_1$ many-electron ground state, angular-dependent photoemission studies by Oelhafen *et al.*[10] find no evidence of the localized Mn $3d$ states in $Cd_{1-x}Mn_xTe$: They concluded that Mn $3d$ states are in fact extended due to a strong hybridization with the Te $5p$ states. The nature of the concentration-independent threshold optical absorption at approximately 2.0—2.3 eV,[22–25] is another controversial issue: It is yet unclear whether it represents an intra-atomic impuritylike transition within the Mn $3d^5$ manifold[22,23] or, like in pure hexagonal MnTe,[26] an interband transition between the occupied Te $5p$ states and the empty Mn $3d$ states.[24,25]

A few electronic structure calculations on pure MnTe have been reported. Czyzyk and Podgorny[27] have calculated the electronic structure of a hypothetical ferromagnetic (F) MnTe in the zinc-blende (ZB) structure using a non-self-consistent mixed basis Gaussian-plane-wave method. Surprisingly, they found that both the Mn spin-up ($d_\uparrow$) and the spin-down Mn ($d_\downarrow$) bands are occupied and situated below the Te $5p$ states. This unusual electronic structure is not supported by any of the self-consistent studies[16,17] including the present one (see Sec. V C). Total energy and band structures[16,17] for both F MnTe and AF MnTe in the ZB structure have been calculated using the augmented-spherical-wave (ASW) method. There are reports also on the band-structure[28,29] and cluster[30] calculations of AF MnTe in the hexagonal NiAs structure. These calculations gave a similar qualitative picture of this material and confirmed the validity of the Allen *et al.* (Ref. 26) qualitative model for the electronic structures of MnTe which describes the valence bands as Te $5p$ + Mn $3d_\uparrow$ state (with the $d_\uparrow$ states embedded in the p states), and the conduction band as a Mn $d_\downarrow$ + Mn $4s$ state. Unfortunately, these calculations[28–30] are all non-self-consistent. In using different fitting parameters or *ad hoc* crystal potentials, these calculations[28–30] result in somewhat different descriptions of the position of the Mn $3d_\uparrow$ and $3d_\downarrow$ bands, the magnitude of the Mn $3d$ exchange splitting, the bandwidth, and the nature of the low-energy excitations. The differences between the band-structure calculations[28,29] and de Groot's (Ref. 30) cluster calculation are particularly large.

We have previously drawn attention[31] to two interesting anomalies in the $A^{II}_{1-x}Mn_xC^{VI}$ system. *First,* whereas most conventional octet isovalent semiconductor alloys retain in solution the underlying crystal structure of their end-point constituents (i.e., zinc-blende, wurtzite, and rocksalt structures for III-V alloys, II-VI alloys, and I-VII alloys, respectively), the $A^{II}_{1-x}Mn_xC^{VI}$ alloys exhibit over a wide composition range the adamantine crystal structure of $A^{II}C^{VI}$, rather than that of MnC^{VI} [rocksalt for MnS and MnSe, and the hexagonal NiAs-type structure for MnTe (Ref. 13)]. *Second,* whereas the band gap of conventional octet isovalent alloys is equal to or smaller than the concentration weighted average $\bar{E}(x)=(1-x)E_{AC}+xE_{BC}$ of the band gaps E_{AC} and E_{BC} of its end-point components, the band gap of $Cd_{1-x}Mn_xTe$ (1.6—2.2 eV) is *larger* than both that of CdTe (1.6 eV at low temperature) or MnTe (1.3 eV). In this paper we explore the nature of these two anomalies and conclude that they share a common physical origin. We suggest that the alloy environment stabilizes an adamantine phase of MnTe, hitherto unknown to exist in its own phase diagram. Considering this phase, together with the ZB structure of CdTe as the appropriate end-point compounds, we find that the concentration variations in the band gaps in the low Mn concentration region and lattice constants are entirely normal. Using the local-spin-density (LSD) (Refs. 32 and 33) total-energy approach, we then proceed to study the electronic and structural properties of the following systems: (i) CdTe, (ii) ferromagnetic (F) and antiferromagnetic (AF) zinc-blende MnTe, (iii) AF MnTe in the NiAs structure, and (iv) F $CdMnTe_2$ as a model for an ordered, 50%-50% alloy of $Cd_{1-x}Mn_xTe$. We show that due to the simultaneous occurrence of localized (nearly unhybridized) Mn $3d$ levels (e states, in crystal-field language) and hybridized Mn $3d$ levels (t_2 states), the optical and photoemission spectra can involve different degrees of orbital relaxation, hence, conventional (unrelaxed) band theory is insufficient to explain the data.

II. STRUCTURE AND BAND-GAP ANOMALIES IN $Cd_{1-x}Mn_xTe$

To appreciate the way in which the structure of $Cd_{1-x}Mn_xTe$ solid solutions differ from those of "conventional" semiconductor alloys, we first survey the latter. We note that an alloy system $A_xB_{1-x}C$, which has some range of mutual solid solubility, is observed to have a single phase with a structure denoted as α at some composition and temperature range $\{T\}$. This alloy can be classified structurally into one of three possible types[31] (Fig. 1):

(i) The alloy is said to be of "type I" if its binary constituents AC and BC both have the structure α as their stable form in the temperature range $\{T\}$. In this case one observes a single Bravais lattice of the type α at all alloy compositions for which solid solubility exists. All isovalent (III-V)—(III-V) semiconductor alloys[11] belong to this class (where α is the zinc-blende phase), and so do most (I-VII)—(I-VII) systems[11] (where α is the rocksalt phase). Figure 1 displays in a matrix form the observed structures of II-VI alloys for which reliable x-ray data exist.[11,34] We see that type-I alloys prevail both for pseudobinary (i.e., common anion or common cation) systems (e.g., ZnS_xSe_{1-x}, $Cd_xHg_{1-x}Te$) as well as for pseudoternary (mixed anion and mixed cation quaternary) systems [e.g., $(ZnTe)_x(CdSe)_{1-x}$] and for systems with complete miscibility range (e.g., $ZnSe_xTe_{1-x}$, HgS_xSe_{1-x}), as well as for systems exhibiting limited solubility (e.g., ZnS_xTe_{1-x}).

(ii) An alloy is said to belong to "type II' if either its AC or its BC components do not have the structure α as

the stable crystal form at the temperature range $\{T\}$ (instead, another phase, i.e., β, is stable there), but the α phase does exist in the phase diagram of the constituents at some different temperature range. In this case one observes the alloy to have a $\alpha \leftrightarrow \beta$ phase transition at some critical composition x_c (which generally depends on the preparation conditions and temperature[34,35]). Correspondingly, the alloy lattice constant and band gaps often show a derivative discontinuity at x_c. Such are the alloy systems (shaded regions in Fig. 1) $(CdS)_x(ZnSe)_{1-x}$ (Ref. 36), $(CdS)_x(ZnTe)_{1-x}$ (Ref. 36), $(CdSe)_x(ZnSe)_{1-x}$ (Ref. 37), $(CdS)_x(CdTe)_{1-x}$ (Ref. 38), and $(CdSe)_x(CdTe)_{1-x}$ (Ref. 39), which all show a transition from the zinc-blende phase to the wurtzite phase at some critical x_c, and at temperatures that are usually well below those necessary to attain a thermodynamically stable wurtzite form for the binaries constituents (e.g., pure CdS becomes wurtzite above 700—800 °C,[36] whereas pure ZnS becomes wurtzite only above 1020 °C).[40,41] It then appears that in type-II alloys the alloy environment stabilizes the high-temperature phase of the constituent binary systems.

(iii) An alloy is said to be of "type III" if either its AC or its BC component do not have in their (zero-pressure) (x,T) phase diagram the structure α which exists in their solid solution. In this case the alloy environment stabilizes a structure which is fundamentally new to at least one of its components. Such is the case (dashed areas in Fig. 1) for $(HgS)_x(CdS)_{1-x}$ (Ref. 42) and $(HgSe)_x(CdSe)_{1-x}$ (Ref. 43) (exhibiting a concentration range where a single-phase wurtzite form exists, whereas HgS and HgSe are not known to have this structural form); $(MnS)_x(CdS)_{1-x}$ (Ref. 44) and $(MnSe)_x(CdSe)_{1-x}$ (Ref. 45) (showing a single-phase rocksalt form which CdS and CdSe do not have); and $(MnTe)_x(ZnTe)_{1-x}$ (Ref. 46) and $(MnTe)_x(CdTe)_{1-x}$ (Ref. 47) (which show a single-phase hexagonal NiAs structure which ZnTe and CdTe do not have, as well as a single-phase zinc-blende structure which MnTe does not have). These type-III alloys hence show at zero pressure some structural forms that either do not exist in the constituents for any pressure (e.g., wurtzite HgS, HgSe or NiAs-type ZnTe, and CdTe), or they exist only at high pressures (e.g., rocksalt CdS and CdSe). Type-III alloys are clearly (Fig. 1) rare. We next survey the experimental data that show $Cd_{1-x}Mn_xTe$ to be a type-III alloy.

Pure MnTe crystallizes below 1040 °C in the hexagonal NiAs structure (space group $p6_3/mmc$, or D_{6h}^4) and transforms to the NaCl structure above this temperature.[48] In the NiAs phase it has a direct band gap[26] of $E_g(\mathrm{MnTe}) = 1.30$ eV and a nearest-neighbor bond length[48] $R(\mathrm{Mn—Te}) = 2.92$ Å. Pure CdTe has the zinc-blende structure (space group $F\bar{4}3m$, or T_d^2). It has a direct band

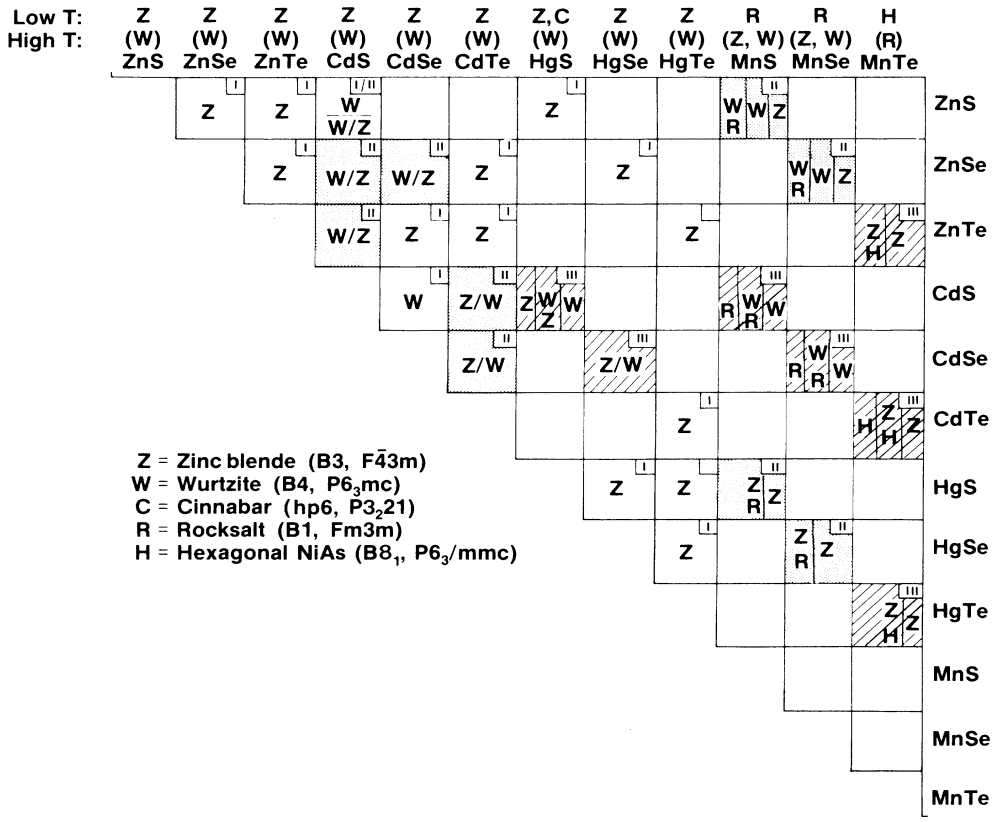

FIG. 1. Observed structures of isovalent II-VI alloys, showing the type-I (blank), type-II (dot-shaded), and type-III (line-shaded) alloys.

gap[49] of E_g(CdTe)=1.59 eV (low-temperature data) and a bond length[50] R(Cd—Te)=2.80 Å. The solid lines in Fig. 2 depict the observed composition variations of the fundamental band gap[6] $E_g(x)$ [Fig. 2(a)] and bond lengths[51] [Fig. 2(b)] in $Cd_{1-x}Mn_xTe$. Expectations based on similar measurements in "normal" (i.e., isovalent octet) semiconductor alloys[52] suggest (dotted lines in Fig. 2) that as Mn is added to CdTe the band gap should *decrease* (with a possible bowing), approaching its smaller value in MnTe, and that the Mn—Te bond length will either *increase* slightly or stay nearly constant[53,54] around its value of 2.92 Å in MnTe. Experimental observations[6,51] (Fig. 2) indicate that instead the opposite is true: for compositions below $x=0.7$, for which single-phase samples can be prepared, the band gap *increases* and the Mn—Te bond length *decreases* slightly with added Mn. A rough extrapolation of the data from $x \leq 0.42$ to $x=1$ (dashed lines in Fig. 2) suggests a "limiting MnTe phase" with a band gap of $E_g \simeq 3.1$ eV and a bond length R(Mn—Te)$\cong$2.73 Å. A similar extrapolation[46,47] for $Hg_{1-x}Mn_xTe$ gives similar values, $E_g \cong 3.3$ eV and R(Mn—Te)$\cong$2.74 Å. The differences between the properties of this "limiting MnTe phase" and those of normal[26,48] MnTe are so dramatic that we are inclined to think that this phase corresponds to a hitherto unknown new structure of MnTe with fundamentally new properties (hence, a "type-III" alloy). This hypothesis is subjected to a first-principles total-energy calculation (Secs. IV and V) and found to be valid.

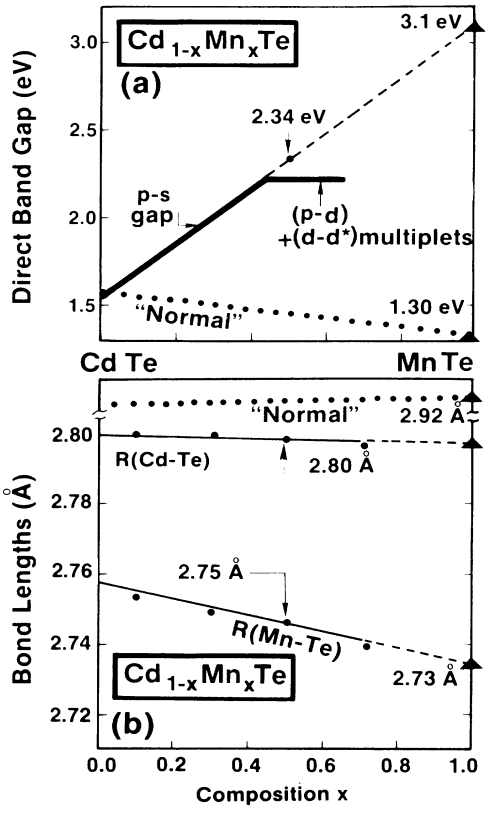

FIG. 2. Observed variations with composition x of (a) the fundamental band gap (Ref. 6) and (b) bond lengths (Ref. 51) in $Cd_{1-x}Mn_xTe$. Dashed lines are extrapolations; dotted lines are expectations for "normal" isovalent alloys.

III. METHOD OF CALCULATION

We use the self-consistent, first-principles, spin-polarized, general-potential linearized augmented-plane-wave (LAPW) method[55] within the local-spin-density-functional formalism.[32,33] The details of this method have been described elsewhere;[55] here, we shall indicate only the aspects of the method pertinent to the present study.

We have included scalar relativistic effects for all valence states (including the Mn $3d$ and Cd $4d$ states). Core states are calculated fully relativistically, retaining only the spherical part of the potential. All core and valence states are treated self-consistently, i.e., without frozen-core approximation. Shape unrestricted potential and charge density and the von Barth—Hedin[33] spin-polarized exchange correlation potential (in the Hedin-Lundquist[33] paramagnetic limit) are used. In the calculation of MnTe in NiAs structure the muffin-tin (MT) radii are 2.71 and 2.80a.u. for the Te and Mn atoms, respectively. A larger Mn MT radius is used to test convergence of the calculated local magnetic moments (defined as an integral of the spin density inside the MT spheres). For all the other calculations, a MT radius of 2.53 a.u. is used for all atoms. The basis set consists of about 90 basis functions per atom. Eigenvalues are converged with respect to the number of basis functions to 1 mRy for all valence bands except the d band, which is converged to approximately 5 mRy. The *absolute* magnitude of the cohesive energy is converged with respect to basis functions to about 0.8 eV/(atom pair) (e.g., extrapolating to an infinite number of basis functions[56] shows the cohesive energy for CdTe and F MnTe to be about 5.4 and 7.7 eV, respectively, compared with the directly calculated values of 4.61 and 7.37 eV, respectively). However, the calculated lattice parameters are unchanged to within ± 0.01 Å by a similar increase in the number of basis functions, and similarly, the magnitude of the *relative* cohesive energies of two phases (a central quantity in the present study) remains stable to within 0.01 eV/(atom pair).

For computational convenience in the AF calculation, we have used the ordinary space group (instead of the magnetic one) by treating the two Mn atoms in the unit cell with opposite spins as two different types of atoms. This reduces the symmetry of the ZB structure from T_d^2 to D_{2d}^5 and that of the NiAs structure from D_{6h}^4 to D_{3d}^3. In the Brillouin zone (BZ) integration we have used two special $\mathbf{k}$ points[57] in the irreducible zone of the ZB structure, and their *equivalent* (i.e., folded-in) $\mathbf{k}$ points for the CuAu-I structure [$\mathbf{k}_1=(2\pi/a)(\frac{1}{4},\frac{1}{4},\frac{1}{4})$ and $\mathbf{k}_2=(2\pi/a)(\frac{1}{4},\frac{3}{4},\frac{1}{4})$ with equal weights]. Considering the small energy difference between the structures and their different Bravais lattices (fcc for F MnTe and CdTe and tetragonal for AF MnTe and $Cd_{1-x}Mn_xTe$), we find that the use of equivalent $\mathbf{k}$ points is necessary to eliminate random errors arising from the $\mathbf{k}$-point sampling. We have tested this construct by performing total-energy cal-

culations for F MnTe both in its two-atom ZB unit cell and in the four-atom CuAu-I unit cell and find the two energies (per atom) to agree within our computational accuracy.

The total-energy calculations for AF MnTe in the NiAs structure are performed only at the experimental lattice constants ($a=4.143$ Å, $c=6.705$ Å),[48] and no attempt is made to minimize the total energy with respect to the numerous structural parameters. In treating the complex band structure of MnTe in the NiAs structure, we found it necessary to use 12 special **k** points.[58] The uncertainty in the total-energy difference between cubic and hexagonal phases due to **k**-point sampling is estimated to be less than 0.1 eV/(atom pair); it is considerably smaller for the energy difference between the ZB and CuAu-I structures [about 0.01 eV/(atom pair)].

Finally, the density of states (DOS) is calculated using the tetrahedral integration method[59] with a square broadening scheme (with a width of 12 mRy). The total DOS and the site and angular momentum projected *local* DOS (LDOS) for each atom is calculated using 8, 12, and 10 uniformly spaced **k** points in the irreducible Brillouin zone for ZB, CuAu-I, and the NiAs structures, respectively. The primary eigenvalues at these **k** points are then used to perform a least-squares fit to a larger set of **k** points (16, 30, 29 **k** points in the irreducible zone for the ZB, CuAu-I, and NiAs structures, respectively) from which the DOS and local DOS are calculated.

IV. TOTAL ENERGIES AND STRUCTURAL STABILITY

We have modeled the 50%-50% $Cd_{1-x}Mn_xTe$ alloy by a ferromagnetic ordered structure (space group D_{2d}^5) whose cation sublattice corresponds to the CuAu-I phase (space group D_{4h}^1). Assuming no tetragonal distortion (i.e., $c=a$),[60] this structure (inset to Fig. 5 below) has the primitive lattice vectors

$$\begin{aligned} \mathbf{a}_1&=(0.5,0.5,0.0)a\ , \\ \mathbf{a}_2&=(-0.5,0.5,0.0)a\ , \\ \mathbf{a}_3&=(0.0,0.0,1.0)a\ , \end{aligned} \tag{1}$$

and the atomic site coordinates

$$\begin{aligned} &\text{Mn at } \tau_1=(0.0,0.0,0.0)a\ , \\ &\text{Cd at } \tau_2=(0.5,0.0,0.5)a\ , \\ &\text{Te at } \tau_3=(0.25,0.25,u)a\ , \\ &\text{Te at } \tau_4=(0.25,0.75,1-u)a\ . \end{aligned} \tag{2}$$

Here, u is a dimensionless "anion displacement parameter." The anion-cation bond lengths (i.e., Cd—Te and Mn—Te) in this structure are related to u by

$$\begin{aligned} R_{AC}&=\tau_1-\tau_3=(u^2+\tfrac{2}{16})^{1/2}a\ , \\ R_{BC}&=\tau_2-\tau_4=[(u-\tfrac{1}{2})^2+\tfrac{2}{16}]^{1/2}a\ . \end{aligned} \tag{3}$$

Hence, in addition to its cubic lattice constant a, the tetragonal structure has an internal structural degree of freedom u, given from Eq. (3) by $u=\frac{1}{4}+(R_{AC}^2-R_{BC}^2)/a^2$ and measuring the possible mismatch in the two bond lengths R_{AC} and R_{BC} in the unit cell. When $u=\frac{1}{4}$, the Mn—Te and Cd—Te bond lengths are equal, as is the case in the ZB structure.

Table I depicts the calculated equilibrium lattice parameters a, bond lengths, and the anion displacement u, compared with the experimental (as well as interpolated) data.[51] Figure 3 depicts the calculated variations with bond length of the total energies of F MnTe and AF MnTe in the ZB structure. Table I lists their ground-state properties. The calculated results for nonmagnetic CdTe are also listed in Table I.

A number of conclusions are apparent from these following results.

(i) the AF phase of cubic MnTe is stabler than the F phase by the spin-polarization-induced ferromagnetic-antiferromagnetic stabilization energy $\Delta E_{\mathrm{MnTe}}^{\mathrm{F,AF}}=-0.19$ eV/(atom pair) (Fig. 4). The two phases have similar bond lengths—R(Mn—Te)$=2.70\pm0.02$ Å—very close to the value of 2.73 Å extrapolated from the experimental data for the "limiting phase" (Fig. 2).[51]

(ii) MnTe in these phases has a substantial cohesive energy [7.37 and 7.56 eV/(atom pair) for the F and AF phases, respectively] relative to those of divalent non-

TABLE I. Calculated ground-state properties of F MnTe, F $CdMnTe_2$, CdTe, and AF MnTe in comparison with experimental data. The calculated cohesive energy for AF MnTe in NiAs structure at $a=4.143$ Å, $c=6.705$ Å is 7.77 eV.

	F MnTe (ZB)		F $CdMnTe_2$ (D_{2d}^5)		CdTe (ZB)		AF MnTe (ZB)	
Property	Calc.	Expt.	Calc.	Expt.	Calc.	Expt.	Calc.	Expt.
a_{eq} (Å)	6.26	6.33[a]	6.37	6.39[b]	6.46	6.48[c]	6.23	6.33[a]
u_{eq}			0.243	0.242[b]				
E_c (eV)/cell	7.37		12.03		4.61	4.12[d]	7.56	
R(Mn—Te) (Å)	2.71	2.73[a]	2.73	2.75[b]			2.70	2.73[a]
R(Cd—Te) (Å)			2.79	2.80[b]	2.80	2.80[c]		

[a]Extrapolated from alloy data to $x=1$, see Fig. 2 and Ref. 51. $T=300$ K.
[b]Alloy data at $x=1/2$, see Fig. 2 and Ref. 51. $T=300$ K.
[c]Reference 50.
[d]Reference 61.

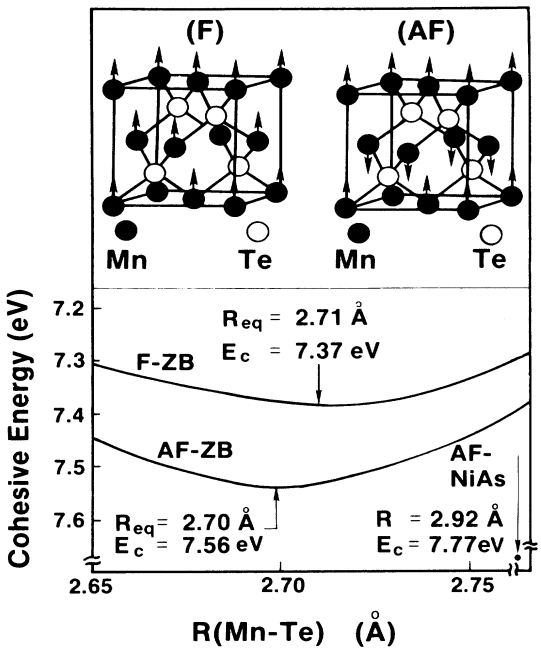

FIG. 3. Cohesive energy as function of zinc-blende lattice parameter for F and AF MnTe, showing the equilibrium values E_c and R_{eq}. The calculated result for AF MnTe in the NiAs structure is shown at its experimental lattice constants (solid circle). The inset depicts the spin ordering in these two phases.

transition-metal tellurides (5.72, 4.56, and 4.12 eV, for MgTe, ZnTe, and CdTe, respectively).[61] This excess stability reflects a balance of two competing effects. *First*, when a solid has spin-unpaired bands, its cohesive energy contains a contribution ΔE_{SP} due to the loss of spin-polarization (SP) energy in transferring the free atom (having localized orbitals) to the solid (having less localized orbitals and hence a smaller spin-polarization energy). This loss of spin-polarization energy[62] ΔE_{SP} is substantial in covalent solids (e.g., MnTe) relative to more ionic solids (e.g., MnS, where the narrower bands imply higher localization and hence a smaller loss of SP energy in the solid relative to the free atoms). Calculated results[62] for the ZnS:Mn, ZnSe:Mn, and GaP:Mn impurity systems indeed indicate ΔE_{SP} to increase with the covalency, being 1.0, 1.2, and 2.5 eV, respectively. Conventional II-VI semiconductors have $\Delta E_{SP}(\text{cation}) \equiv 0$ on account of their closed shells. This effect alone would then lead to a *larger* cohesive energy in Mg, Zn, and Cd tellurides relative to MnTe. *Second*, the availability of five additional chemically active ($3d^5$) electrons in Mn compounds relative to Mg, Zn, and Cd compounds implies an *increased* cohesion in the former. Contrary to the ΔE_{SP} effect, the covalent gain in cohesive energy *increases* with the system's covalency, since it makes the d orbitals more potent as sources of binding. This second effect overwhelms the first one for these systems, as evidenced by the fact[63] that Mn chalcogenides have a cohesive energy that exceeds that of Cd and Zn chalcogenides by 1—3 eV. This analysis is discussed further in the Appendix.

(iii) We find that the *observed* NiAs structure of MnTe is stabler by the hexagonal-cubic stabilization energy (Fig. 4) $\Delta E^{ZB,H}_{MnTe} = -0.40 \pm 0.1$ and -0.21 ± 0.1 eV/(atom pair) relative to the zinc-blende F and AF forms, respectively. Hence, we do not expect to find the isolated ZB phase under conditions where equilibration to the NiAs form is not hindered by kinetic activation barriers.

(iv) By fitting the total energy $E[\text{CdMnTe}_2, a, u]$ as a quadratic function of u and a, we find at equilibrium $a_{eq} = 6.370$ Å and $u_{eq} = 0.243$. These values correspond to R(Mn—Te)$=2.73$ Å and R(Cd—Te)$=2.79$ Å, which are within 1% of the values observed for the 50%-

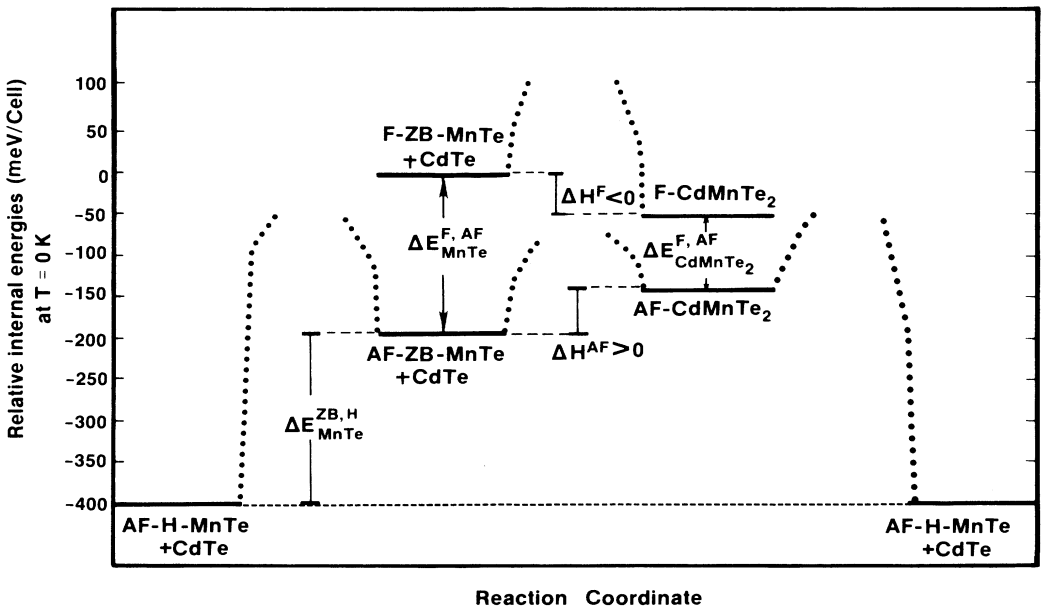

FIG. 4. Relative total energies (thick horizontal lines) of some possible structural and magnetic phases of the MnTe + CdTe system. Dotted lines indicate schematically possible activation barriers.

50% alloy in extended x-ray-absorption fine-structure (EXAFS) measurements.[51] The nonideal anion displacement ($u \neq \frac{1}{4}$) in the F $CdMnTe_2$ structure (i.e., the Te anion moves away from the center of its tetrahedron toward the pair of Mn atoms and away from the pair of Cd atoms) leads to the formation of Mn—Te and Cd—Te bond lengths similar to what is found in the respective binary systems [R^0(Mn—Te)=2.71 Å and R^0(Cd—Te)=2.80 Å, calculated for pure F MnTe and CdTe, respectively (Table I)], but considerably different from what a virtual-lattice approximation (VLA) would have predicted [i.e., $u=\frac{1}{4}$ and $R^{(\mathrm{VLA})}$(Mn—Te)$=R^{(\mathrm{VLA})}$(Cd—Te)$=\sqrt{3}/4a=2.758$ Å]. The fact that our calculated equilibrium bond lengths are close to those of the pure end-point compounds indicates that the system has used its internal degree of freedom u to achieve nearly ideal tetrahedral bond lengths (at the expense of somewhat distorting the bond angles), thereby lowering its strain energy. The same effect was observed to occur in all $A^{\mathrm{I}}B^{\mathrm{III}}C_2^{\mathrm{VI}}$ chalcopyrite crystals[54] as well as in the 50%-50% alloy system GaP-InP.[53]

(v) We evaluate the enthalpy of formation (per four atoms) $\Delta H^{(\mathrm{F})}$ for the ferromagnetic phases relative to the equilibrium ZB forms of CdT and F MnTe as

$$\Delta H^{(\mathrm{F})}=E[\text{F CdMnTe}_2]-E[\text{CdTe}]-E[\text{F MnTe}] . \quad (4)$$

For the AF phase we have the formation enthalpy

$$\Delta H^{(\mathrm{AF})}=E[\text{AF CdMnTe}_2]-E[\text{CdTe}]-E[\text{AF MnTe}] . \quad (5)$$

We find a *negative value* of $\Delta H^{(\mathrm{F})}=-0.05\pm0.01$ eV (Fig. 4). Hence, *the ordered CuAu-I phase of F $CdMnTe_2$ is predicted to be stable against disproportionation into its ZB constituents.* Bonding with CdTe thus reduces the metastability barrier of F-ZB-MnTe.

(vi) In contrast, we find that because of the large AF stabilization of MnTe relative to the F phase [$\Delta E^{\mathrm{F,AF}}_{\mathrm{MnTE}}=-0.19$ eV/(atom pair)], $\Delta H^{(\mathrm{AF})}$ is *positive* (at least $+0.04$ eV/(atom pair)].[64] This is so because the AF stabilization of the mixed $CdMnTe_2$ compound ($\Delta E^{\mathrm{F,AF}}_{\mathrm{CdMnTe_2}}$) is *smaller* than the AF stabilization in pure MnTe on account of the more dilute magnetic interactions (i.e., fewer nearest-neighbor Mn atoms and a larger Mn-Mn interatomic distance).

Figure 4 summarizes our calculated total-energy differences (solid horizontal lines) relative to the pair [F-ZB-MnTe + CdTe] used as a reference energy. These calculated total energies suggest a number of observations on the relative stabilities of the various species. *First,* if complete thermodynamic equilibrium can exist in the alloy between all of its constituents, the system at $T=0$ K will separate into hexagonal MnTe plus CdTe, which are the lowest energy species. *Second,* in actuality one might expect strong elastic activation barriers[53] (depicted schematically in Fig. 4 by the dotted lines) against disproportionation of an alloy with a lattice constant $a(Cd_{1-x}Mn_xTe)$ to its constituents having radically different lattice constants (Table I). If one then considers such a constrained "equilibrium," then the only ordered phase possible at $x=\frac{1}{2}$ is F $CdMnTe_2$, on account of its $\Delta H^{(\mathrm{F})}<0$, which makes its disproportionation into F-ZB-MnTe + CdTe unfavorable. This phase could spontaneously (activationlessly) become antiferromagnetic (since AF $CdMnTe_2$ has a lower energy than F $CdMnTe_2$ by $\Delta E^{\mathrm{F,AF}}_{\mathrm{CdMnTe_2}}$); however, once formed, AF $CdMnTe_2$ might disproportionate into its *stabler* constituents AF-ZB-MnTe + CdTe (since $\Delta H^{(\mathrm{AF})}>0$). This suggests that such *Mn-rich alloys* might in fact show clustering of AF MnTe domains with strongly coupled Mn atoms.[3,65] While the measurement of the $Cd_{1-x}Mn_xTe$ phase diagram indicates multiple-phase regions only for $x>0.7$, our calculation suggests that a precursor of such a phase (in the form of clustering of MnTe) could exist already at $x\sim0.5$. At very low x values, the Mn and Cd distributions are essentially random.[65] *Third,* at finite temperatures the *disordered* alloy gains stability on account of its negative entropy term $-T\Delta S$; hence, above some critical temperature T_c it will be the stablest species. It is likely that conventional growth temperatures exceed T_c; hence, only a disordered, quenched-in phase is formed. At low temperatures and slow growth rates, the $x=\frac{1}{2}$ alloy might produce a crystallographically ordered $CdMnTe_2$ stable compound. Furthermore, recent theoretical studies on epitaxial confinement[66] suggest that if the alloy is grown on a substrate with a different lattice constant, substrate strain effects may further stabilize the ordered phase. Experimental attempts to grow and characterize such potentially *ordered* structures and examine the possibility of clustering at high Mn concentrations are called for.

Our total-energy calculation thus points to the existence of an alloy-stabilized ZB phase of MnTe, hitherto unknown to exist in its own phase diagram, with a bond length which is in excellent agreement with that inferred for the "limiting phase" from the data on $Cd_{1-x}Mn_xTe$ [Fig. 2(b)]. We now proceed to investigate the electronic structure of the F $CdMnTe_2$, cubic MnTe, CdTe, and hexagonal MnTe phases.

V. BAND STRUCTURE AND DENSITY OF STATES

A. Ferromagnetic $CdMnTe_2$ and the negative exchange splitting

The spin-polarized band structure of F $CdMnTe_2$ at the lattice constant $a=6.255$ Å, and $u_{\mathrm{eq}}=0.242$ is depicted in Figs. 5(a) and 5(b) for spins up and down, respectively. The total and partial density of states within the atomic muffin-tin spheres are depicted in Fig. 6. Because of the restriction to nonoverlapping muffin-tin spheres and the nonuniqueness of the partitioning of space into such spherical objects, the site-projected local DOS is obviously not a unique quantity. Nevertheless, it serves as a qualitative description of the atomic and orbital origins of the various band states.

The lowest valence band in this system is constituted primarily from Te s orbitals, with a minor Cd character. The next highest band is the Cd d band which peaks at $E_v^{\uparrow}-9.2$ eV and $E_v^{\downarrow}-7.5$ eV [where $E_v^{\uparrow}$ and $E_v^{\downarrow}$ denote the

TABLE II. Atomic energy levels (in eV) from LSD semirelativistic calculation using the von Barth and Hedin exchange correlation.

	Configuration	Spin-up orbital energy	Spin-down orbital energy
Mn $3d$	$3d^5_+4s^2$	−8.41	−4.16
Mn $4s$		−5.82	−4.69
S $3s$	$3s^2 3p^3_+ 3p^1_-$	−18.07	−16.29
S $3p$		−7.84	−6.23
Se $4s$	$3d^{10}4s^2 4p^3_+ 4p^1_-$	−18.14	−16.70
Se $4p$		−7.30	−5.92
Te $5s$	$4d^{10}5s^2 5p^3_+ 5p^1_-$	−16.11	−15.00
Te $5p$		−6.66	−5.52

valence-band maxima (VBM) for spin up and spin down, respectively]. We see that the upper valence-band complex has a Mn d and Te p characteristic, which differs widely for spin up and spin down. Regarding its d components, we find that the spin-up Mn d band is occupied [Fig. 6(b)] and centered at $E_v^{\uparrow}-3.7$ eV, whereas the spin-down d band is empty [Fig. 6(b)] and centered at $E_v^{\downarrow}+2.9$ eV. The $+4.9$ eV separation between them constitutes the effective d band exchange (x) splitting $\Delta_x(d)$, depicted in Fig. 6(b). We find, however, that another important exchange splitting exists in the problem—the p-d exchange splitting $\Delta_x(pd)=E_v^{\downarrow}-E_v^{\uparrow}$ of the top of the

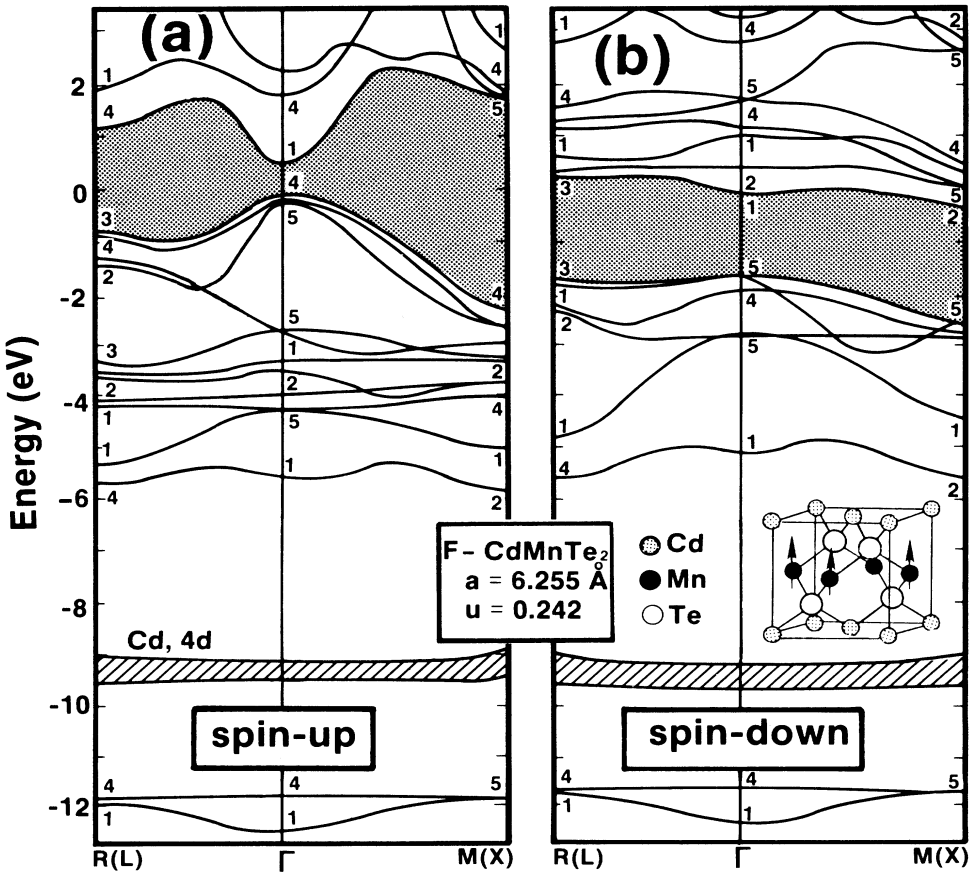

FIG. 5. Electronic band structure of F $CdMnTe_2$. (a) Spin up. (b) Spin down. The zero of the energy is at $E_v^{\uparrow}$. Symbols in parentheses are the points of fcc BZ. The band-gap regions are shaded.

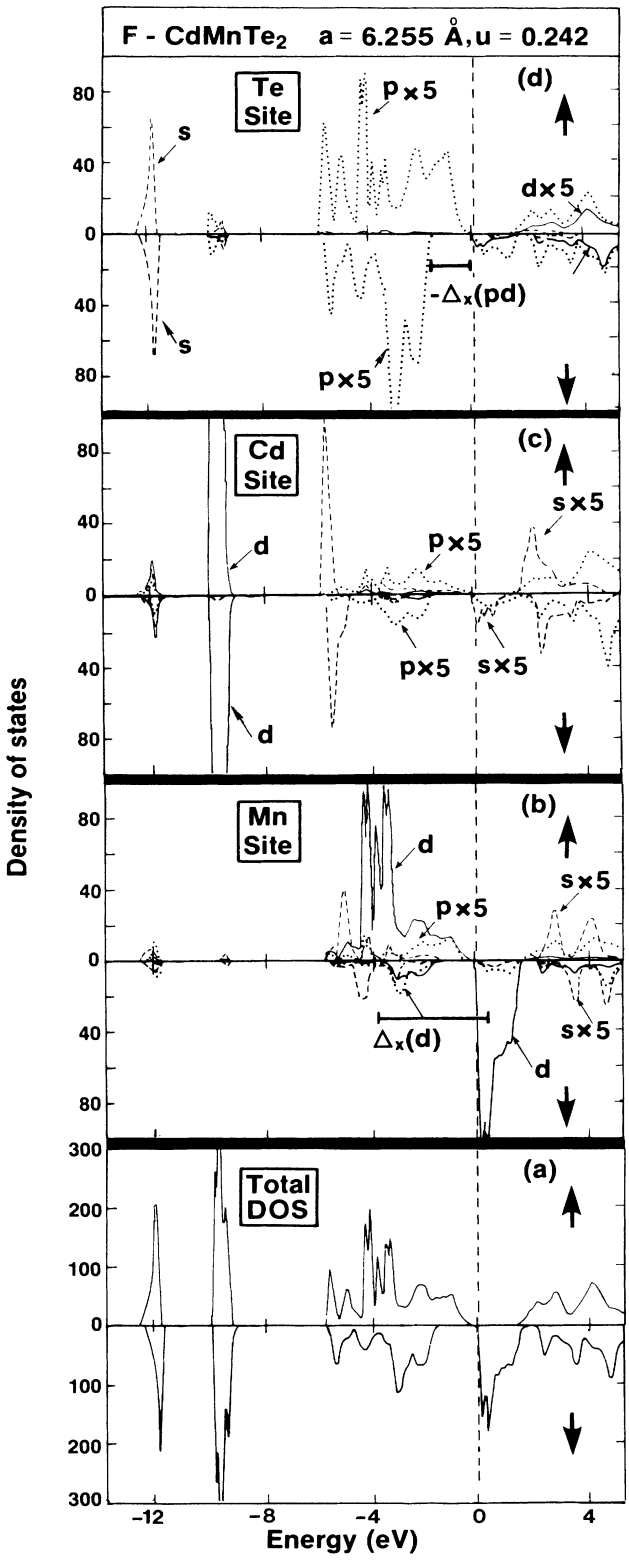

FIG. 6. Total density of states (DOS) (a) and angular momentum and site projected local DOS (b)—(d) of F $CdMnTe_2$ with spin up and spin down. Zero energy is at $E_v^{\uparrow}$.

valence bands for spin up [Figs. 5(a) and 6(d)] and spin down [Figs. 5(b) and 6(d)]—and that it is *negative*: the top of the valence band for spin up ($E_v^{\uparrow}$) is 1.7 eV *above* the top of the valence band for spin down ($E_v^{\downarrow}$). This is at first surprising, given that we find the effective potential for the minority spin to be more attractive than that for the majority spin, as is usually the case in spin polarized systems.[67] Figure 7 explains this phenomenon in terms of a simple *p-d* repulsion model.[54] What is special about Mn and Te atoms (as well as the pairs Mn—S and Mn—Se) is that the calculated $p_{\uparrow}$ and $p_{\downarrow}$ orbital energies (Table II) of the anion are bracketed by the atomic $d_{\uparrow}$ and $d_{\downarrow}$ levels of the cation. Indeed the atomic exchange splitting of Mn $3d$ is far larger (4.25 eV) than that of S, Se, and Te valence p orbitals (1.61, 1.38, and 1.14 eV, respectively). We depict this situation in Figs. 7(a) and 7(b). In the tetrahedral crystalline environment, the anion p states transform as the $t_2(\Gamma_{15})$ representation, whereas the cation d states are split into a doublet $e(\Gamma_{12})$ representation and a triplet $t_2(\Gamma_{15})$ representation. In substitutional T_d symmetry, the e states are lower in energy than the t_2 states.[12] This is depicted in Fig. 7(c). Since the Mn $3d$ e states transform differently from the Te $5p$ states, there is no *p-d* hybridization in this (Γ_{12}) channel, and hence the e_+ and e_- states are essentially unperturbed in the solid [Fig. 7(d), we return to this point in Sec. VI]. On the other hand, the interaction between the anion and cation spin-up states of the same t_2 symmetry produces a lower bonding (B_+) and a higher antibonding (AB_+) band. Similarly, the coupling between the anion and cation spin-down states with the same t_2 symmetry produces a lower bonding (B_-) and a higher antibonding (AB_-) pair of bands [Fig. 7(d)]. The *order* of these levels can be gathered from the atomic energy levels discussed above: Since the unperturbed atomic $d_{\uparrow}$ is lower in energy than $p_{\uparrow}$, but $d_{\downarrow}$ is above $p_{\downarrow}$ [Table II and Fig. 7(c)], simple perturbation theory[54] leads to a situation in which B_- is below AB_+; hence, we have an effective *negative p-d* exchange splitting. This *p-d* coupling mechanism has been used previously[54] to explain the anomalously small band gaps of ternary $3d$ semiconductors. It also suggests here a smaller spin-up band gap (calculated: 0.63 eV) than the spin-down band gap (1.64 eV), since AB_+ is repelled upward relative to B_-. We therefore predict that a spin-polarized photoemission experiment for F $Cd_{1-x}Mn_xTe$ will show the emission of majority spin states (AB_+) at *lower* binding energies than that of the minority spin (B_-). This picture is substantiated by an inspection of the calculated charge density at $E_v^{\uparrow}$ and $E_v^{\downarrow}$, shown in Fig. 8. It indicates that $E_v^{\uparrow}$ is a strong *antibonding* AB_+-like state with a node along the Mn—Te bond [Fig. 8(a)], whereas $E_v^{\downarrow}$ is a *bonding* B_--like state [Fig. 8(b)]. The existence of a negative exchange splitting has not been recognized in the energy-level diagram proposed recently by Taniguchi *et al.*[68] (see their Fig. 6): They include a B_+ and AB_+ bands and the narrow e_+ band between them, but they missed B_-. The large *p-d* hybridization is also responsible to the smaller spin-orbit splitting Δ_0 of $Cd_{1-x}Mn_xTe$ (since d states have negative spin-orbit splitting). Calculated Δ_0 values are 0.87 and 0.63 eV for CdTe and ZB MnTe, respectively (see below).

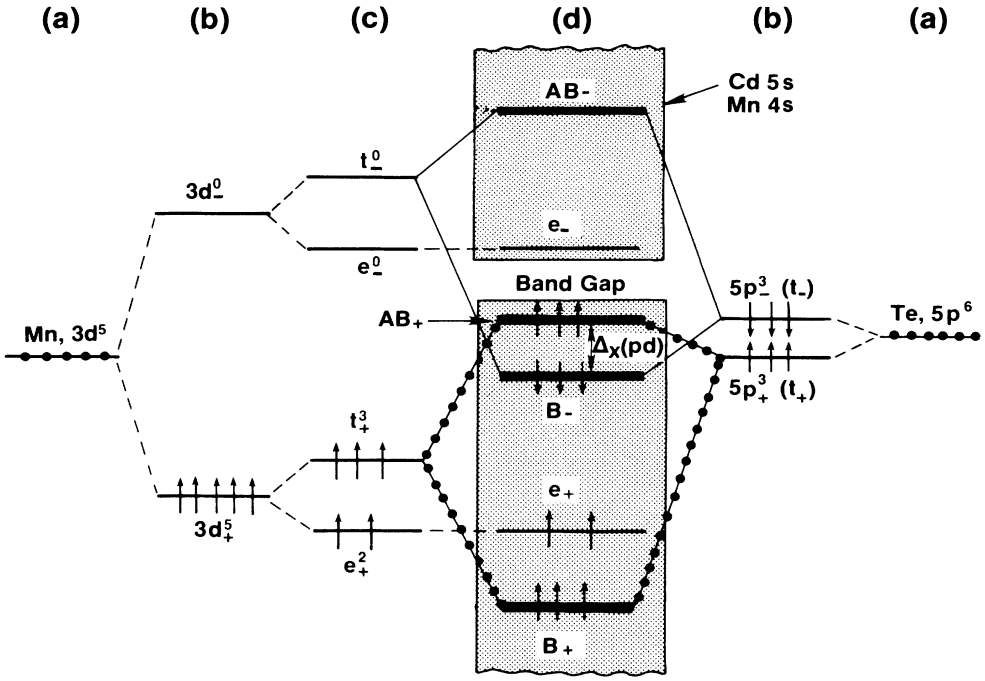

FIG. 7. A schematic diagram of the p-d repulsion effects for a ferromagnetic system with anion p states bracketed by the cation d states. (a) shows the atomic unpolarized levels, (b) shows the exchange-split atomic levels, (c) shows the crystal-field split levels, and (d) shows the final interacting states. Shaded areas denote the host crystal bands.

B. CdTe

To see the relationships between F $CdMnTe_2$ and its end-point compounds F MnTe and CdTe, we calculated the band structures of CdTe and F MnTe as well as F $CdMnTe_2$ at their respected experimental bond lengths,[51] i.e., R(Cd—Te)=2.80 Å and R(Mn—Te)=2.75 Å (see Fig. 2). In this way, we eliminate any inconsistencies in the comparison due to lattice relaxation. Eigenvalues at the Γ point of the CuAu-I structure are listed in Table III. Since states at the Γ point in the CuAu-I Brillouin zone are folded from $\Gamma+X$ in the fcc BZ, we list in Table III the Γ and X ZB levels as well. In the CuAu-I structure Γ_{15} states of the fcc BZ split into $\Gamma_4+\Gamma_5$ (the latter is doubly degenerate), and Γ_{12} states in the fcc BZ split into $\Gamma_1+\Gamma_2$ states in the tetragonal lattice.

Figure 9 gives the band structure of CdTe along the L-Γ-X lines. Figure 10 shows the calculated total and partial DOS of CdTe. The CdTe valence band can be divided into three parts: (i) the band centered at $E_v-11.3$ eV with a bandwidth of 0.49 eV, which originates from the Te 5s orbitals; (ii) the narrow Cd 4d bands at $E_v-8.5$ eV

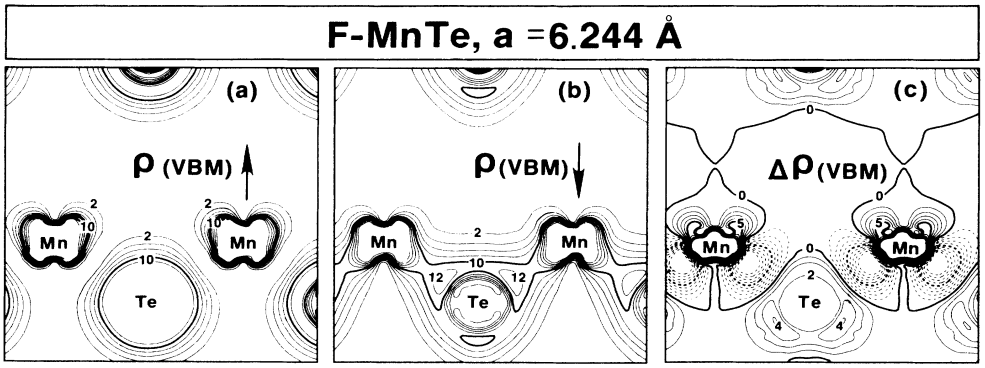

FIG. 8. Charge density plots of the states at the VBM in F-ZB-MnTe in the (110) plane; (a) spin up (AB_+); (b) spin down (B_-); (c) the difference between spin up and spin down. Dashed lines indicate a negative value. The charge density is given in units [10^{-3} e/(a.u.)^3]; the step size is 2 for (a) and (b) and 1 for (c).

TABLE III. Eigenvalues ε (in eV) and angular momentum decomposed charge inside the muffin-tin spheres (in percentage) of F-ZB-MnTe, F $CdMnTe_2$, CdTe, and AF-ZB-MnTe at the Γ point of the tetragonal BZ. R(Cd—Te)=2.80 Å, R(Mn—Te)=2.75 Å, and R_{MT}=1.339 Å for all the atoms. Symmetry notation for tetragonal lattice is used. The symbols in parentheses are the corresponding points in the zinc-blende BZ. For the paramagnetic or AF phase, the zero energy is at the VBM. For the F phase, the zero energy is midway between $VBM_\uparrow$ and $VBM_\downarrow$. For each state the first row is for the Te atom, the second row for Mn [or Mn(1)] atoms and the third row is for Cd [or Mn(2)] atoms. Cd 4d states are not listed in this table.

	F-ZB-MnTe ↑				$CdMnTe_2$ ↑				CdTe				$CdMnTe_2$ ↓				F-ZB-MnTe ↓				AF-ZB-MnTe			
States	ε	s	p	d	ε	s	p	d	ε	s	p	d	ε	s	p	d	ε	s	p	d	ε	s	p	d
Γ_{1v}	−10.88	63	0	0	−11.13	63	0	0	−11.30	62	0	0	−10.98	63	0	0	−10.59	65	0	0	−10.84	64	0	0
(Γ_{1v})		8	0	0		3	0	0						3	0	0		6	0	0		4	0	0
						4	0	0		8	0	0		4	0	0						3	0	0
Γ_4	−10.03	72	0	0	−10.51	64	0	0	−10.80	61	0	0	−10.40	63	0	0	−9.78	74	0	0	−10.03	73	0	0
(X_{1v})		0	3	3		0	1	1						0	1	1		0	2	2		0	1	1
						0	1	12		0	2	16		0	1	13						0	1	1
Γ_{1v}	−4.05	0	27	0	−4.23	0	27	0	−4.45	0	25	1	−3.83	1	30	0	−3.22	0	34	0	−3.69	0	30	0
(X_{3v})		16	0	16		9	0	7						8	0	1		15	0	4		8	0	11
						13	0	2		28	0	3		16	0	2						7	0	2
Γ_{5v}	−3.27	0	16	0	−3.08	0	18	0													−2.91	0	17	0
(Γ_{15v})		0	0	69		0	1	65														0	1	66
						0	0	0														0	0	1
Γ_{4v}					−2.83	0	12	0													−2.73	0	15	0
						0	0	70														0	0	64
						0	0	1														0	1	3
Γ_{2v}	−2.40	0	0	1	−2.36	0	0	0													−2.13	0	0	0
(Γ_{12v})		0	0	93		0	0	93														0	0	93
						0	0	0														0	0	0
Γ_{1v}					−2.31	0	2	2													−1.97	0	3	1
						2	0	83														3	0	81
						3	0	0														2	0	0
Γ_{5v}	−1.02	0	29	0	−1.56	0	40	0	−1.92	0	43	0	−1.72	0	45	0	−1.38	0	45	0	−1.58	0	44	0
(X_{5v})		0	8	30		0	4	9						0	5	9		0	8	9		0	3	1
						0	6	2		0	10	2		0	4	0						0	5	12
Γ_{5v}	1.28	0	46	0	0.69	0	49	0	0.00	0	56	0	−0.70	0	41	0	−1.28	0	38	0	0.00	0	25	0
(Γ_{15v})		0	3	29		0	2	19						0	0	22		0	1	34		0	3	26
						0	1	3		0	4	7		0	3	4						0	0	22

TABLE III. (*Continued*).

States	F-ZB-MnTe ↑				$CdMnTe_2$ ↑				CdTe				$CdMnTe_2$ ↓				F-ZB-MnTe ↓				AF-ZB-MnTe			
	ε	*s*	*p*	*d*	ε	*s*	*p*	*d*	ε	*s*	*p*	*d*	ε	*s*	*p*	*d*	ε	*s*	*p*	*d*	ε	*s*	*p*	*d*
Γ_{4v}					0.70	0	49	0					−0.90	0	36	1					−0.44	0	20	1
						0	2	19						0	0	29						0	2	18
						0	1	3						0	2	2						0	0	32
Γ_{1c}													0.87	3	1	2					1.13	0	0	2
														0	0	60						4	0	0
														10	0	0						2	0	73
Γ_{2c}													1.33	0	0	0	1.29	0	0	1	1.27	0	0	1
(Γ_{12c})														0	0	89		0	0	87		0	0	0
														0	0	0						0	0	88
Γ_{4c}													2.15	1	20	2					2.43	1	23	2
														0	3	33						0	0	14
														0	1	4						0	3	25
Γ_{5c}													2.55	1	20	0	3.48	0	25	0	2.87	0	23	0
(Γ_{15c})														0	1	63		0	1	62		0	0	0
														0	1	4						0	1	58
Γ_{1c}	1.99	24	0	0	1.14	22	1	0	0.44	24	0	0	1.72	20	3	0	3.06	20	0	0	2.49	21	0	0
(Γ_{1c})		25	0	0		11	0	0						9	0	14		22	0	0		13	0	0
						19	0	0		38	0	0		12	0	0						11	0	1
Γ_{4c}	3.05	6	0	5	2.80	5	0	4	2.45	4	1	3	3.56	5	2	3	4.41	6	0	3	4.01	5	3	3
(X_{1c})		0	10	12		0	5	5						0	1	31		0	7	34		0	6	2
						0	7	2		0	14	4		0	9	1						0	1	36

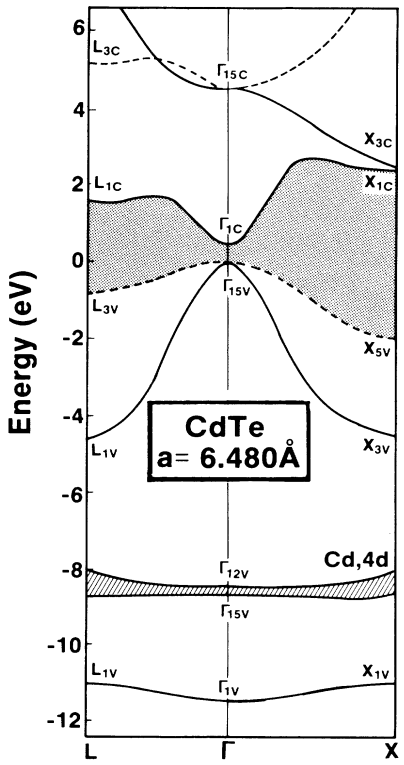

FIG. 9. Electronic band structure of CdTe. The band-gap region is shaded. Dashed lines indicate doubly degenerate states.

TABLE IV. Comparison of high-symmetry band eigenvalues (in eV) of CdTe for $a=6.480$ Å of the present study with the recent LMTO results of Cade and Lee (fully relativistic). Our scalar relativistic (SR) results are also listed (with notation). The Hedin-Lundqvist exchange correlation potential is used.

State	LMTO[a] (R)	LAPW (R)	LAPW (SR)
Γ_{6v}	−11.63	−11.59	−11.30 (Γ_{1v})
Γ_{8v}	−8.1	−9.21	−8.61 (Γ_{15v})
Γ_{7v}		−8.66	
Γ_{8v}	−7.6	−8.46	−8.36 (Γ_{12v})
Γ_{7v}	−0.95	−0.87	
Γ_{8v}	0.0	0.0	0.0 (Γ_{15v})
Γ_{6c}	0.47	0.15	0.44 (Γ_{1c})
Γ_{7c}	3.94	3.94	
Γ_{8c}	4.30	4.29	4.46 (Γ_{15c})
$X_{6v'}$		−11.11	−10.81 (X_{1v})
$X_{7v'}$	−4.72	−4.76	−4.46 (X_{3v})
X_{6v}	−2.40	−2.38	
X_{7v}	−2.03	−2.04	−1.92 (X_{5v})
X_{6c}	2.15	2.16	2.45 (X_{1c})
X_{7c}	2.24	2.24	2.52 (X_{3c})
$L_{6v''}$		−11.21	−10.92 (L_{1v})
$L_{6v'}$	−4.86	−4.86	−4.55 (L_{1v})
L_{6v}	−1.41	−1.35	
$L_{4,5v}$	−0.84	−0.83	−0.80 (L_{3v})
L_{6c}	1.43	1.29	1.57 (L_{1c})
$L_{6c'}$	4.93	4.77	
$L_{4,5c}$	5.11	4.93	5.14 (L_{3c})

[a]Reference 69.

with a bandwidth of 0.77 eV at Γ; and (iii) the upper Te $5p$ + Cd $5s$ valence band, with a bandwidth of 4.6 eV. The calculated direct band gap at Γ ($\Gamma_{15v}\rightarrow\Gamma_{1c}$) is 0.44 eV, considerably smaller than the experimental value 1.6 eV.[49] Table IV compares our results at some high-symmetry points with those of Cade and Lee,[69] who have used the linear muffin-tin orbital (LMTO) method. Since their calculation is fully relativistic, we have also performed a calculation for CdTe, including spin-orbit coupling for the valence states. We find good agreement between the two calculations. Our calculated positions of Cd $4d$ states ($\approx E_v-8.5$ eV for the semirelativistic case and $E_v-9.0$ eV after including spin-orbit coupling) is about 1–2 eV higher than the experimental result.[70] The reason for this underestimation[71] is that the one-electron picture neglects a core-hole relaxation effects and other many-body effects, which are significant for localized states. These corrections deepen the one-electron binding energy.

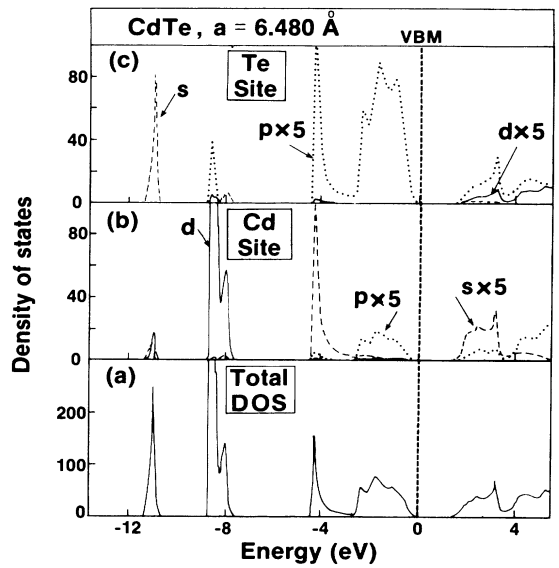

FIG. 10. Total DOS (a) and angular momentum and site-projected local DOS (b) and (c) of CdTe. Zero energy is at the VBM.

C. F MnTe in the zinc-blende structure

Figures 11(a) and 11(b) depict the band structure of F-ZB-MnTe at $a=6.244$ Å. Similar to the situation encountered for F $CdMnTe_2$, we find that p-d repulsion here too causes a negative p-d exchange splitting of −2.56 eV (Table III) and a reduction in the spin-up band gap (0.71 eV) relative to the spin-down band gap (2.57 eV). Interestingly, this effect is so pronounced in F-ZB-MnTe that $E_c^{\downarrow}$ (with a minimum at the X point) is *below* $E_v^{\uparrow}$ (maximum at the Γ point), producing an *overall* metallic character despite the semiconductive character of each of the *individual* spin directions. We find that the spin-up Mn d band F MnTe is occupied, 1.2 eV wide, and centered at $E_v^{\uparrow}-4.2$ eV, whereas the spin-down d band is empty, 2.6 eV wide, and centered at $E_v^{\downarrow}+3.8$ eV. The

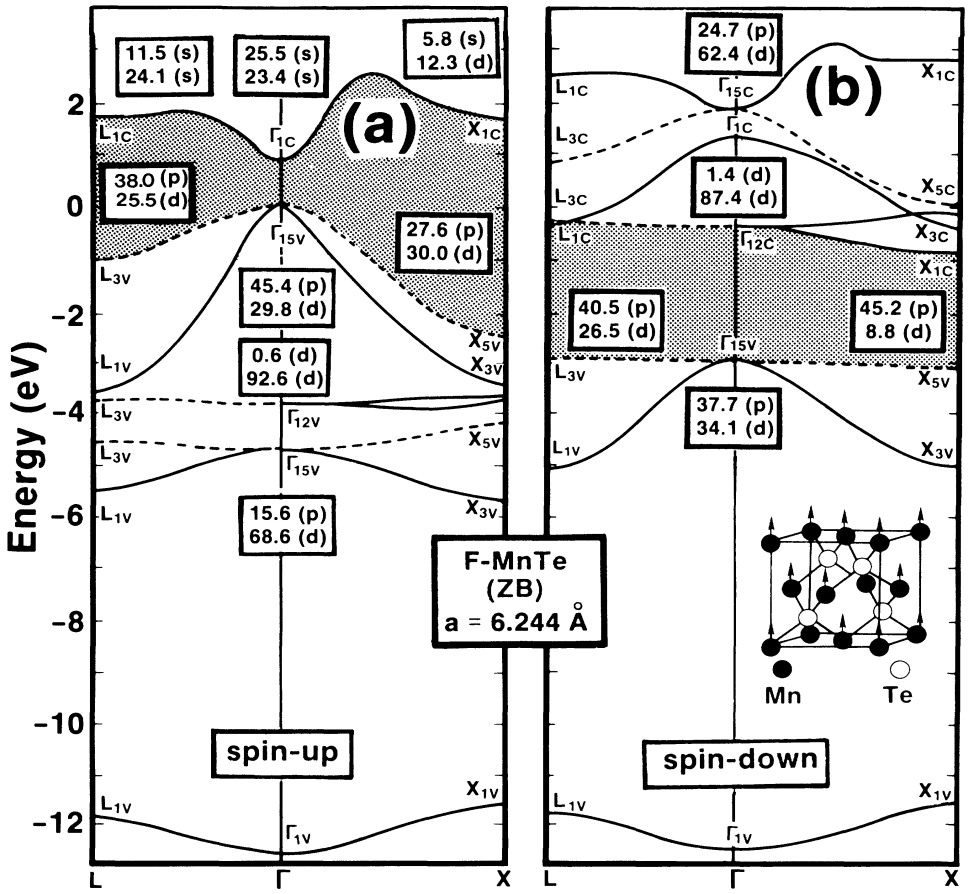

FIG. 11. Electronic band structure of F-ZB-MnTe (a) and (b). The inset depicts the spin ordering of this phase. Numbers in the boxes are the percentage l character within the muffin-tin spheres for Te and Mn atoms (see also Table III).

+ 5.4 eV separation between them constitutes the effective d band exchange splitting $\Delta_x(d)$, which is positive.

It is interesting to compare our band structure for F-ZB-MnTe with the previous non-self-consistent calculations of Czyzyk and Podgorny (CP),[27] using a mixed basis approach. A schematic comparison of the electronic levels at the Γ point is depicted in Figs. 12(a) and 12(b). One astonishing result from their calculations is that they found both Mn $3d_\uparrow$ and Mn $3d_\downarrow$ states to be occupied, leading to an effective "Mn d^{10}" configuration, and consequently, the system is metallic [Fig. 12(a)]. Since both Mn $3d$ states are below the Te $5p$ states, no negative exchange splitting $\Delta_x(pd)$ is found in their calculation. This surprising result is in obvious contradiction with our calculation, in which we find only Mn $3d_\uparrow$ states to be occupied and, for individual spin direction, the system to be a semiconductor. We believe that this pathology in their results may reflect a combination of the inadequacy of their input *ad-hoc* charge density (the positions of transition-metal d bands depend strongly on self-consistency) and the artificially large exchange coefficient they used (which spuriously deepens localized states such as the Mn d bands).

Hass *et al.*[17] have calculated the band structure of ZB-F-MnTe in the Γ-X direction using the ASW method. Their results appear generally similar to ours (no details

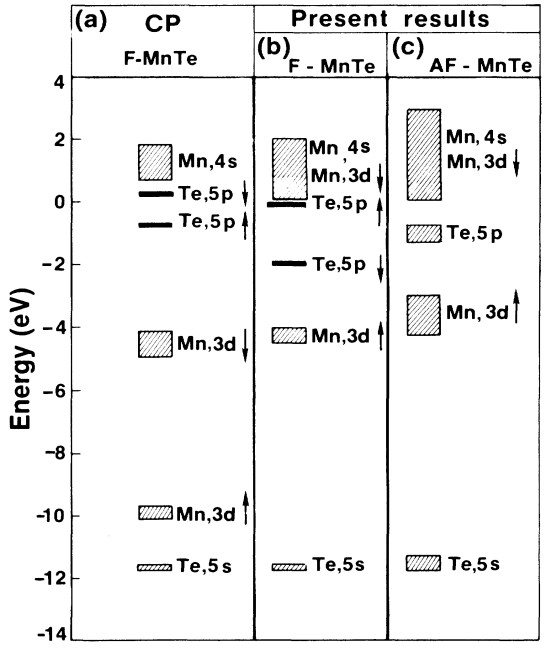

FIG. 12. Comparison of our self-consistently calculated eigenvalues of F-ZB-MnTe at the Γ point (b) with that of Ref. 27 (a). Our results for AF-ZB-MnTe are shown in (c).

are given, unfortunately in Ref. 17), except for an upwards shift of their s-like conduction bands, presumably because of omission of relativistic effects.

D. Comparison of CdTe, F MnTe, and F $CdMnTe_2$ band structure: Optical bowing

Comparing the band eigenvalues of CdTe, F MnTe, and F $CdMnTe_2$ (Table III), we find that introducing Mn into CdTe has little effect on states that are localized on the Te and Cd atoms (e.g., Te $5s$, Cd $4d$ states). Furthermore, the energy levels of $CdMnTe_2$ can be predicted within a few tenths of an eV by averaging the corresponding energy levels of the end-point compounds CdTe and F MnTe (Table III), implying a small optical bowing in $CdMnTe_2$. For instance, we find the calculated interband p-s transition $[(\Gamma_{4v}^{\uparrow},\Gamma_{5v}^{\downarrow})\rightarrow\Gamma_{1c}]$ to be at 1.43 eV;[72] this value is close to the average (1.485 eV) of our calculated p-s ($\Gamma_{15v}-\Gamma_{1c}$) transition energies of the end-point compounds; i.e., $E^{p\text{-}s}$(CdTe)=0.44 eV and $E^{p\text{-}s}$(F MnTe)=2.53 eV,[72] indicating a small optical bowing for $Cd_{1-x}Mn_xTe$ if the *correct* MnTe phase is used (i.e., ZB, not NiAs). This result also implies that while the absolute values of LSD band gaps cannot be meaningfully compared with experiment, their relative magnitudes are more realistic.[54]

VI. AF-ZB-MnTe

To see the effects of the AF ordering of Mn atoms on the electronic band structure, we performed a band structure calculation for the zinc-blende MnTe with the first kind of AF order, i.e., with successive (001) planes aligned antiferromagnetically (see the inset to Fig. 13). Figure 13 shows the band structure of AF-ZB-MnTe at $a=6.244$ Å. The density of states of AF-ZB-MnTe is shown in Fig. 14. Eigenvalues at Γ points, calculated for the experimental lattice constant,[51] are given in Table III. We find the occupied "spin up" (i.e., first Mn sublattice) Mn d band to be centered at $E_v-2.5$ eV, whereas the empty, "spin-down" (i.e., second Mn sublattice) d band is centered at $E_v+2.2$ eV; hence, the exchange splitting is $\Delta_x(d)\simeq+4.7$ eV (smaller than in F MnTe; see Fig. 11). The valence-band maximum is strongly hybridized, having a $2\times12.6\%$ Te p character and about a 24% Mn d character on each of the Mn sublattice. The bottom of the conduction band is almost dispersionless. The direct band gap at Γ is 1.13 eV, which is 0.9 eV *larger* than the one we calculate for the NiAs structure of MnTe realized at point A (see below), confirming our expectation based on Fig. 2(a). Our calculation indicates that AF-ZB-MnTe is a semiconductor rather than a metal, because the intra-atomic exchange splitting for the Mn ion is large enough to keep the unoccupied spin states above the top of the Te p bands. The AF ordering increases the band gap. In contrast with the ferromagnetic case, there is no negative p-d exchange splitting and band overlap of $E_v^{\uparrow}$ and $E_c^{\downarrow}$ (where v stands for valence band and c for conduction band) in the AF spin arrangement. This is so because in the AF phase there is an equal number of Mn atoms with $3d$ levels below and above the Te p levels (compare, however, the ferromagnetic case in Fig. 7). The latter are re-

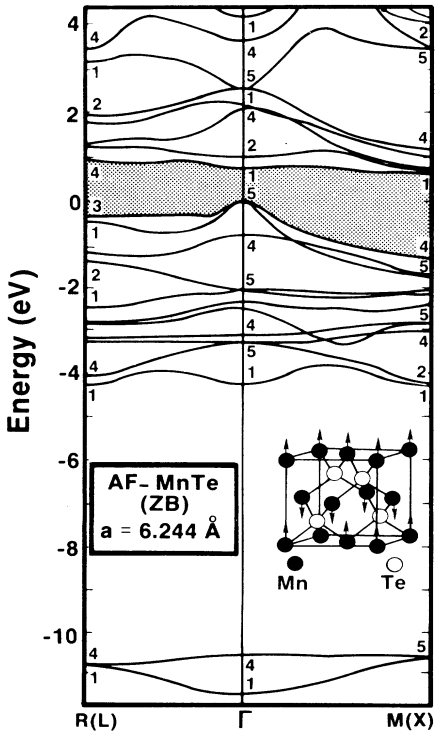

FIG. 13. Electronic band structure of AF-ZB-MnTe. The zero of the energy is at the VBM.

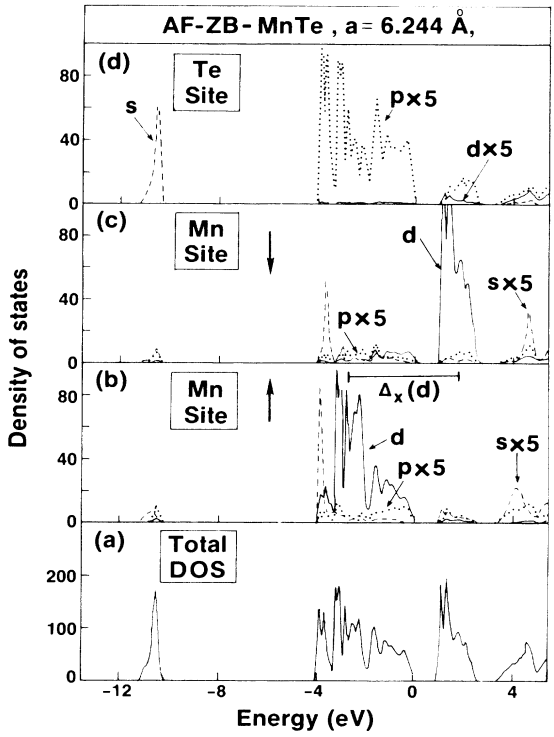

FIG. 14. Total DOS (a) and angular momentum and site projected local DOS (b)—(d) of AF-ZB-MnTE.

pelled equally by $d_\uparrow$ and $d_\downarrow$; hence, *no exchange splitting occurs for the Te p bands.* Because of this p-d repulsion, a red shift and a smaller blue shift are expected to occur for F and AF magnetic ordering, respectively, relative to the magnetically disordered phase. Furthermore, since, in the AF ordering, states at the valence-band edge are more bonded, the difference in spin symmetry between the F and AF phases also indicates the enhanced stability of the AF structure (Fig. 4): the p-d repulsion in the F phase reduces the cohesion of the p bands.

Comparing the band eigenvalues of F MnTe and AF MnTe in the ZB structure (Table III), we see that (i) for all the states except the Mn d states, the average of spin-up and spin-down eigenvalues of F MnTe is very close to the value of corresponding states in the AF MnTe; (ii) the exchange splitting of Mn $3d$ states is smaller in AF phase than in the F phase. This means that both spin-up and spin-down Mn $3d$ states are closer to the VBM in the AF phase, increasing thereby the p-d hybridization. Our comparison indicates that it is possible to predict the general features of the band structure of a more complicated AF arrangement from the simpler F phase by a proper averaging of the corresponding states. This method is adopted in this study to find the location of Mn $3d_\uparrow$ states of non-spin-polarized $Cd_{1-x}Mn_xTe$ from the calculated F $CdMnTe_2$ band structure. We find it to be at about $E_v-2.5$ eV.

Our band structure of AF MnTe in the hypothetical ZB structure also exhibits a global similarity to that calculated by Larson *et al.*[16] The main difference is in the position of the Mn $4s$ conduction band. Larson *et al.*[16] find this state to be well above the unoccupied Mn $3d_\downarrow$ states, whereas our calculation finds this state to overlap with the Mn $3d_\downarrow$ bands. Similar to the F-ZB-MnTe case, this difference is due to their omission of relativistic effects.

VII. ELECTRONIC EXCITATIONS AND IONIZATIONS

Considerable controversy exists in the literature regarding the nature of the optical transitions in $Cd_{1-x}Mn_xTe$ for $x>0.4$, at the 2.0–2.3 eV energy range [Fig. 2(a)]. These sharp transitions, observed in piezomodulation[7] and reflectivity[8] in $Cd_{1-x}Mn_xTe$ as well as in $Zn_{1-x}Mn_xTe$ (2.33–2.40 eV; see Ref. 9), have been interpreted as intra-atomic $d\rightarrow d^*$ multiplet transitions of the ${}^6A_1\rightarrow{}^4T_1,{}^4T_2$ type[7–9,22,23] as well as interband transitions.[24,25] Such localized excitations are known from the spectra of dilute Mn impurities in II-VI semiconductors,[12] e.g., the ${}^6A_1\rightarrow{}^4T_1$ (${}^4T_2$) transitions occur at 2.34 (2.53), 2.31 (2.47), and 2.30 (2.40) eV in ZnS:Mn, ZnSe:Mn, and ZnTe:Mn, respectively. The similarity of the transition energies in the alloy to those of the impurity systems, as well as the near-composition-independence of the transition energy [Fig. 2(a)], has been used to support the interpretation of $d\rightarrow d^*$ excitations. On the other hand, Grancharova *et al.*[25] have argued that these transitions represent interband excitations and that the true $d\rightarrow d^*$ transitions are expected to occur at higher energies ($\sim$2.4 eV), but are not observed.

It appears to us that much of the confusion in this area results from the failure to properly recognize the strong dependence of the system's energy on its electronic configuration and occupations. Such strong dependences (i.e., correlation effects) characterize systems that sustain localized states;[12] they vanish in the one-electron band-structure model for *extended* states. Such orbital relaxation effects are well known in atomic physics, where the ionization energy (the difference between the total energy of the system with N electrons and that with $N-1$ electrons) are known to differ considerably from the orbital energy of the N-electron system (by a correction to the Koopmans theorem). The notion of a "rigid-band structure," i.e., the association of excitation energies to various possible final states with a single band structure (of the ground state), rests on the hope that relaxation effects are either negligible (free-electron systems), or are approximately equal for all final states. None of these expectations hold in $Cd_{1-x}Mn_xTe$, which not only shows localized states, but also exhibits variable degrees of localizations in the valence band. We illustrate this point in the *schematic energy-level diagram* depicted in Fig. 15.

The ground state of the neutral system involves the Mn^{2+} formal oxidation state in which the e_+ and t_+ states of Fig. 7 are fully occupied. We consider here only low-energy excitations; hence, we simplify in Fig. 15 the notation of Fig. 7 to include only the e_+, t_+, and e_- levels of Fig. 7. (The e_+ level is analogous to the e^{CFR} "crystal field resonance" familiar[12] from the impurity physics, and the t_+ level is similarly the t_2 "dangling-bond hybride," or DBH, in impurity systems.) Hence, the ground state of the neutral system [Fig. 15(b)] is denoted as $[Mn^{2+},d^5,e_+^2t_+^3e_-^0,{}^6A_1]$.

A. Ionization

The ith orbital ionization energy of an N-electron system can be generally calculated as the difference in total energies of the final ($N-1$ electrons) and initial systems[73]

$$E^{(N-1)}-E^{(N)}=-[\varepsilon_i^{(N)}+\Delta_i(N,N-1)]\ . \tag{6a}$$

In the absence of relaxation effects (Koopmans limit in Hartree-Fock theory), this equals simply the negative of the orbital energy $-\varepsilon_i^{(N)}$ of the initial system; otherwise, a general state i-dependent relaxation-polarization correction $\Delta_i(N,N-1)$ exists.[73] In conventional band theory one assumes $\Delta_i(N,N-1)=0$ for all i's. Whereas it has been recognized that $\Delta_i(N,N-1)$ can be very large in isolated atoms and ions, it has been generally expected that effective screening in the final state in solids will render $\Delta_i(N,N-1)$ small, or at least constant (i.e., i independent). It is now clear[71,73] that this expectation does not hold for a large class of solids or for deep impurities in covalent semiconductors. A useful approximation of (6a) exists in local density theory (the "transition state" construct[74]), whereby Eq. (6a) can be written as

$$\varepsilon_i^{(N)}+\Delta_i(N,N-1)\cong\varepsilon_i^{(N-0.5)}\ , \tag{6b}$$

i.e., using an occupation number intermediate between the initial (N) and final ($N-1$) states.

For Mn in $Cd_{1-x}Mn_xTe$ one has a broad $d_\uparrow$ band (Figs. 5 and 6), hence a number of possible final-state con-

figurations for ionization. The two limiting situations[12] (in crystal-field language) involve ionizations from either the t_+ or the e_+ orbitals. In the former case, the final state can be denoted formally as $[Mn^{3+},d^4,e_+^2t_+^2e_-^0F^1,{}^5T_2]$ (where the final-state orbital F—a conduction or vacuum level, is occupied) whereas in the latter case we have $[Mn^{3+},d^4,e_+^1t_+^3e_-^0F^1,{}^5E]$. Our discussion of Sec. V A emphasized the significant difference between the two cases: whereas the t_+ orbital is hybridized with the host crystal (p-d mixing being allowed in the t_2 representation of T_d), the e_+ orbitals are essentially nonbonding (no p-d coupling for the e representation is allowed in T_d symmetry). As we ionize t_+^3 [Fig. 15(b)] to t_+^2 [Fig. 15(a)], the orbital energy drops, as we have relieved part of the Coulomb repulsion (even though the reduced exchange splitting will move the bands up). The ionization energy relative to the valence-band maximum ε_v in this donorlike transition is

$$\Delta E_t(0/+)=E[Mn^{3+}]-E[Mn^{2+}] \cong\{\varepsilon_v-\varepsilon_{t_+}\}_{e_+^2t_+^{2.5}F^{0.5}} . \quad (6c)$$

The observed Mn d value[68] is at about $\varepsilon_v-3.5$ eV. In our calculation $\varepsilon_{t_+}^{(N)}\cong\varepsilon_v-(2.0\text{—}2.5$ eV), hence the relaxation shift is $\Delta_t(N,N-1)\cong-(1\text{—}1.5$ eV). The reason that this shift is so much smaller than in the free Mn^{2+} ion[12,75] is related to the effective screening of the t_+ hole in the solid: similar calculations for $3d$ impurities in semiconductors[12] have shown that the hybridized host crystal resonances respond to the creation of a hole in a localized t orbital by increasing the amplitude of their wave function on the impurity site, thereby returning to it much of its charge lost in the ionization process (the "self-regulating response"[12,76]). Hence, whereas in *occupation number space* we have a $d^5\rightarrow d^4$ transition, in *coordinate space* we have a $L^Md^5\rightarrow L^{M-1}d^5$ transition, where the ligands (L, initially with M electrons) have lost approximately one electron and the impurity site remained essentially neutral "charge transfer" excitation.[12] This process is not to be confused with ordinary dielectric screening (returning $1-1/\epsilon$ electrons to the ionized site, where ϵ is the dielectric constant) which occurs on a far larger distance scale (a few, not one bond length), and is unrelated to the details of the hybridization.

At the extreme limit when an e_+ electron, rather than a t_+ electron, is ionized, we have instead of Eq. (6c)

$$\Delta E_e(0/+)\cong\{\varepsilon_v-\varepsilon_{e_+}\}_{e_+^{1.5}t_+^3F^{0.5}} . \quad (6d)$$

Since the e_+ orbital is nonbonding, the self-regulating response is not operative (only ordinary dielectric screening is available), hence the relaxation correction $\Delta_e(N,N-1)$ is expected to be much larger; rigid-band theory is entirely inadequate to explain such transitions. Here, the transition is $L^Md^5\rightarrow L^Md^4$ both in occupation number space and in coordinate space. The recently observed[68] resonant photoemission transition at approximately ε_v-7 eV is hence interpreted as this type of excitation.

We have so far considered the limits of *pure* t_+ and e_+ excitations. In actuality the $d_\uparrow$ band is dispersed and contains a continuous mixture of orbital representations. In addition, alloy disorder acts to further intermix such states, implying coupling of ${}^5T_2$ and ${}^5E$-type final states. Further quantitative (supercell) studies are necessary to clarify this point.

B. Intra-d excitations

In contrast to ionization transitions, intra-center transitions are charge-conserving. Their energy is

$$E_j^{(N)}-E_i^{(N)}=[\varepsilon_j^{(N)}-\varepsilon_i^{(N)}]+\Delta_{ij}(N) , \quad (7a)$$

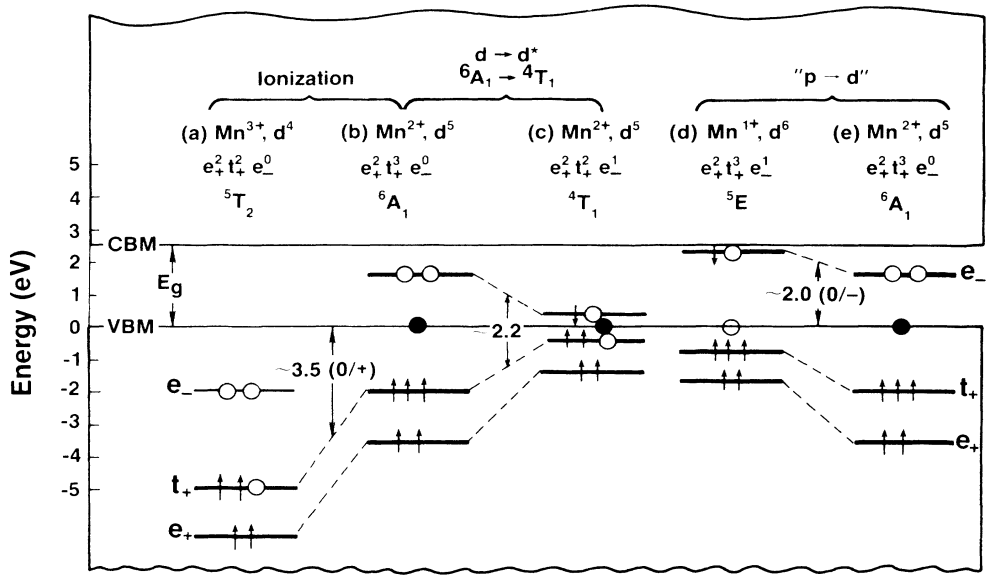

FIG. 15. Energy-level scheme depicting various transitions in Mn-rich $Cd_{1-x}Mn_xTe$. Open circles denote holes.

where we have transferred an electron from the ith orbital to the jth orbital, both in the N-electron system. The excitation relaxation correction $\Delta_{ij}(N)$ can be far smaller than the ionization relaxation-polarization correction $\Delta_i(N,N-1)$, since in the former case the orbital j still has an amplitude on the excited site, and can screen it.

When we excite $[Mn^{2+},d^5,{}^6A_1]$ into its lowest energy, many-electron state we remove an electron from t_+ of $[Mn^{2+},d^5,{}^6A_1]$ and place it in the lowest unoccupied Mn orbital, which is e_-, thereby creating $[Mn^{2+},d^5,e_+^2t_+^2e_-^1,{}^4T_1]$ (higher multiplets, e.g., ${}^4T_2,{}^4E,{}^4A_1$ are possible, too[60]). In this transition [Fig. 15(c)] the exchange splitting in the maximum spin ($S=\frac{5}{2}$) ${}^6A_1$ configuration is reduced ($S=\frac{3}{2}$) in the ${}^4T_1$ configuration; hence, the formerly unoccupied e_- orbital moves *down* in energy. The excitation energy is given by the transition-state construct as

$$\Delta E({}^6A_1\rightarrow{}^4T_1)=\{\varepsilon_{e_-}-\varepsilon_{t_+}\}_{e_+^2t_+^{2.5}e_-^{0.5}} . \tag{7b}$$

We interpret this as the 2.2 eV transition observed[77] in $Cd_{1-x}Mn_xTe$, similar to the values observed in the ZnS:Mn, ZnSe:Mn impurity systems.[12] Because of the p-d hybridization, this transition also has some Te p character.

C. p-d excitations

We can also conceive of a transition in which a valence-band electron is added to the lowest unoccupied Mn orbital [a "Te $p\rightarrow$Mn $d_\downarrow$" transition; Figs. 15(d) and 15(e)]. Here, we create the ground state of Mn^{1+}, i.e., $[Mn^{1+},d^6,e_+^2t_+^3e_-^1,{}^5E]$, plus a hole in the valence band. This acceptorlike transition has the energy

$$\begin{aligned}\Delta E_e(0/-)&=\Delta E(Mn^{2+}/Mn^{1+})\\&=\{\varepsilon_{e_-}-\varepsilon_v\}_{e_+^2t_+^3e_-^{0.5}V^{M-0.5}} ,\end{aligned} \tag{8}$$

where the valence band initially had M electrons. In this case the e_- orbital of Mn^{2+} moves on account of its increased Coulomb repulsion and its lower spin ($S=\frac{4}{2}$), and hence smaller exchange splitting, but not as much as in the ${}^4T_1$ case [Fig. 15(c)], which has an even smaller spin $S=\frac{3}{2}$. We interpret the $\sim$2.0 eV transition observed in luminescence[21] and photoconductivity[78] as this transition (not as a Stocks shifted $d\rightarrow d^*$ transition). Because of the large mixing of Te p and Mn d states at the VBM, this transition also has some $d-d^*$ character.

A few observations are in order. *First,* since the $p\rightarrow d$ transition can occur at slightly lower energies ($\sim$2 eV) than the $d\rightarrow d^*$ transition ($\sim$2.2 eV), the failure to observe Zeeman splitting for the former[77] may simply be due to the masking of the $p\rightarrow d^*$ transition by the $d-d^*$ transition (the expected Zeeman splitting of $\sim$0.05 eV at $B=15$ T is far smaller than the spectral width, see Fig. 2 of Ref. 77). *Second,* the assumption of Vecchi *et al.*[21] that the Mn $d_\uparrow$ bands occur at the same energy in ionization and $d\rightarrow d^*$ excitation is clearly invalid, in view of the large occupation-dependent relaxation effects. *Third,* the occurrence of the donor level (0/+) at $E_v-3.5$ eV and the ${}^4T_1$ state just above the VBM is in agreement with the "vacuum pinning rule,"[71] which places the donor level in ZnS:Mn, ZnSe:Mn, and CdTe:Mn at a similar distance from the vacuum level in all cases. *Fourth,* the ${}^6A_1\rightarrow{}^4T_2,{}^4E,{}^4A_1$ excitations observed[12] in ZnS:Mn and ZnSe:Mn are masked in $Cd_{1-x}Mn_xTe$ by the valence-to-conduction transitions.

D. The Mott-Hubbard Coulomb energy

The Mott-Hubbard Coulomb energy is defined[12] as the energy required to ionize an atom and place the electron on a distant identical atom. This corresponds to the difference between acceptor and donor energies, both referred to the same band edge. In the present system this is

$$\begin{aligned}U(e_-t_+)&=\Delta E_e(0/-)-\Delta E_t(0/+)\\&=(\varepsilon_v+2.0)-(\varepsilon_v-3.5)=5.5\text{ eV} ,\end{aligned} \tag{9a}$$

$$\begin{aligned}U(e_-e_+)&=\Delta E_e(0/-)-\Delta E_e(0/+)\\&=(\varepsilon_v+2.0)-(\varepsilon_v-7)=9.0\text{ eV} .\end{aligned} \tag{9b}$$

Notice that we are transferring in Eq. (9a) an electron from a t_+ orbital to an e_- orbital or [Eq. (9b)] from e_- to e_+; hence, $U(e_-t_+)$ receives a contribution from the crystal field *and* exchange splittings (unlike the d^3-d^4-d^5 case), whereas $U(e_-e_+)$ has a larger relaxation contribution. These large Coulomb correlation energies are the reason why simple, one-electron (occupation-independent) considerations are invalid in this system.

VIII. AF-HEXAGONAL MnTe: LOCALIZED EXCITATIONS IN $Cd_{1-x}Mn_xTe$ AND ITINERANT EXCITATIONS IN MnTe

There is a substantial difference in the absorption spectra[7–9] of $Cd_{1-x}Mn_xTe$ and that of hexagonal (H) MnTe:[26] whereas $Cd_{1-x}Mn_xTe$, as well as Mn impurities in II-VI compounds,[12] shows evidence of localized $d\rightarrow d^*$ excitations at 2.2–2.3 eV [Fig. 2(b), and see the discussion in Sec. VII], the absorption spectra of H-MnTe shows[26] a simple band-to-band character. It is remarkable that both the alloy and the impurity system show localized intra-atomic multiplet excitations, whereas H-MnTe (which has an even larger Mn—Te bond length than the alloy and hence better isolates the Mn site from its ligand atoms; cf. Fig. 2) does not. We will analyze this difference here by inspecting the band structure of the NiAs-type MnTe. Figure 16 depicts the band structure of the hexagonal AF MnTe along some symmetry direction. Table V lists eigenvalues at the Γ point and selected eigenvalues near the band gap at the A and L points and their local charge distributions. The crystal structure of hexagonal MnTe with AF spin ordering is shown in the inset of Fig. 16. In our calculation, the two Mn atoms with opposite spins are treated as different atoms and are designated as Mn(1) and Mn(2). In characterizing band symmetry we have followed the notation of Mattheiss.[79]

The valence bands of the AF-H-MnTe can be divided into two parts. *First,* the two low-lying bands originate from the Te 5s orbitals, are centered at $E_v-11.8$ eV, and

TABLE V. Eigenvalues ε (in eV) and l-decomposed local-charge character (in percentages) of AF MnTe in the NiAs structure at $c=6.705$ Å, $a=4.143$ Å with $R_{MT}(Mn)=1.48$ Å and $R_{MT}(Te)=1.434$ Å. The l character is given first for Te (first line), then for Mn(1) (second line) and for Mn(2) (third line). Symmetry notation is the same as Ref. 79. Zero energy is at VBM (Γ_3^+ state).

State and energy ε	Percentage l character s	p	d	State and energy ε	Percentage l character s	p	d
Γ_1^+ −12.68	66	0	0	Γ_3^+ 0.32	0	0	1
	6	0	0		0	0	1
	5	0	0		0	0	88
Γ_2^- −11.43	78	0	0	Γ_1^+ 0.48	0	1	1
	0	3	0		0	0	8
	0	2	0		2	0	79
Γ_1^+ −5.96	0	34	0	Γ_1^+ 1.78	29	0	0
	12	0	5		24	0	0
	10	0	1		18	0	0
Γ_3^+ −3.83	0	18	0	Γ_3^+ 1.86	0	27	1
	0	0	67		0	0	8
	0	0	3		0	0	54
Γ_1^+ −3.15	0	1	1	A_3^+ 0.0	0	54	0
	2	0	83		0	0	24
	0	0	5		0	4	0
Γ_3^+ −3.10	0	0	1	A_2^- 0.21	3	2	2
	0	0	93		0	2	0
	0	0	1		5	0	71
Γ_3^+ −1.36	0	24	2	A_3^- 0.24	0	0	2
	0	0	24		0	0	0
	0	0	37		0	0	86
Γ_3^- −0.91	0	67	1	L_1^+ −0.72	4	32	0
	0	5	0		1	0	40
	0	4	0		0	5	0
Γ_2^- −0.72	0	70	0	L_2^- −0.19	0	1	3
	0	4	0		0	3	0
	0	3	0		0	0	73

have a bandwidth of 1.5 eV. *Second*, the upper Te $5p$ and Mn $3d$ hybridization bands have a bandwidth of 6.0 eV. The valence-band-maximum occurs at point A in the zone, and the bottom of the conduction band is at L. This agrees with previous calculations[28,29] and expectations from experiment[26] in which a large absorption below the optical edge of 1.3 eV and low resistivity indicates that an indirect band gap exists. The occupied Mn $3d$ states with high LDOS are located near the center in the p-d manifold and at $E_v-3.2$ eV. The unoccupied Mn $3d$ states are located at $E_v+0.8$ eV. This picture is in qualitative agreement with the model proposed by Allen *et al.*,[26] except that our calculated exchange splitting (4.0 eV) is considerably larger than what they proposed (2.1 eV).[26] Because our calculated magnetic moment is smaller than the observed value ($4.17\mu_B$ rather than the $4.7\mu_B$ observed experimentally[80]), our calculated exchange splitting of the Mn $3d$ states (4.0 eV) is relatively small. This reduces the band gap and causes a small, indirect overlap of the valence and conduction bands (0.19 eV). We found that increasing the magnetic moment artificially to $\sim 5.0\mu_B$ can open up this band gap (Table VI). Unlike the previous non-self-consistent calculations,[28] which have adjusted the parameters of the calculation to obtain a direct band gap at L of about 1.3 eV, we find the direct band gap of 0.21 eV is realized at the A point instead. The smallest direct band gap still occurs at the same position even if a large magnetic moment is used (Table VI), since increasing the magnetic moment raises the bottom of the conduction band almost uniformly (see Table VI). The calculated direct transition energies at L and Γ are 0.53 and 1.04 eV, respectively. The calculated indirect band gap (−0.19 eV in the present LSD approach) is 0.4 eV smaller than the direct band gap. The bottom of the conduction bands are almost pure Mn $3d$ "down" states with small dispersion, and the top of the valence bands are the Te $5p$ states with a smaller p-d hybridization than their ZB phase.

We believe that the reason for the absence of localized atomiclike $d \rightarrow d^*$ transitions in AF-H-MnTe is contained in the smaller p-d hybridization in this material relative to its cubic modification and the smaller band gap of H-MnTe. This can be appreciated as follows. Many electron multiplet states within a d^N subshell are caused

TABLE VI. Energy band gap (in eV) of AF MnTe in NiAs structure as function of input local magnetic moment (in Bohr magneton μ_B) with $R_{MT}(Mn)=1.48$ Å (non-self-consistent calculation).

Transition	E_g ($\mu=4.07$)	E_g ($\mu=4.17$)	E_g ($\mu=4.7$)	E_g ($\mu=5.5$)
Γ_{2v}^{-}-Γ_{3c}^{+}	0.92	1.05	1.16	1.69
A_{3v}^{+}-A_{2c}^{-}	0.06	0.21	0.30	0.71
L_{1v}^{+}-L_{2c}^{-}	0.42	0.53	0.68	1.07
A_{3v}^{+}-L_{2c}^{-}	−0.31	−0.19	−0.09	0.30
A_{3v}^{+}-Γ_{3c}^{+}	0.21	0.33	0.49	1.00

by the electron-electron coupling of the various one-electron configurations constructed by distributing N electrons in the various partners of d^N. The strength of this coupling depends both on "covalency" (which dilutes the d character of the orbital by mixing in different, more spatially extended components) and on the site symmetry (a low site symmetry splits the tenfold degeneracy of the atomic $|d\rangle$ states; the split partners then interact more weakly via interelectronic couplings than the degeneracy partners). In *free 3d ions* there is no covalency and no symmetry lowering, hence there are pronounced multiplet effects. In *3d impurity ions in ionic oxides* there is little covalency but a somewhat reduced symmetry (d splits into the sixfold degenerate t_{2g} and the fourfold degenerate e_g components). This somewhat reduces multiplet couplings relative to free ions. In *3d impurities in cubic (zinc-blende) semiconductors* these effects are reduced further by the greater covalency of the matrix, but noticeable multiplet effects are still evident.[7–9,12] Furthermore, p-d hybridization is prevalent, since the $t_2(d)$ orbital can couple with the anion $t_2(p)$ orbital of the same symmetry. In *hexagonal MnTe* we encounter a situation of *covalency at low symmetry,* where most of the atomic degeneracy of the $3d$ orbit is removed by the low site symmetry, leaving little symmetry lowering to multiplet interactions. Indeed in AF MnTe in the NiAs structure, the Mn d states at Γ split into Γ_3^+, Γ_1^+, Γ_3^+, for both spin directions, and the Te p states split into Γ_3^-, Γ_1^+, Γ_2^-, and Γ_3^+ (compare this with the splitting into just $\Gamma_{15}+\Gamma_{12}$ for Mn d and Γ_{15} for Te p states in the tetrahedral field).

Note that although the Te $5p$ Γ_3^+ states are hybridized, the existence of Mn $3d$ states with Γ_3^+ symmetry both below and above it confine the state and do not permit a large shift to occur. Because of their different spatial properties, the Γ_2^-, Γ_3^- states do not mix with Mn $3d$ states. This causes the valence-band-edge states at Γ (with Γ_2^- symmetry) to be pure p-like. At the A point (for convenience, we consider only one spin direction in

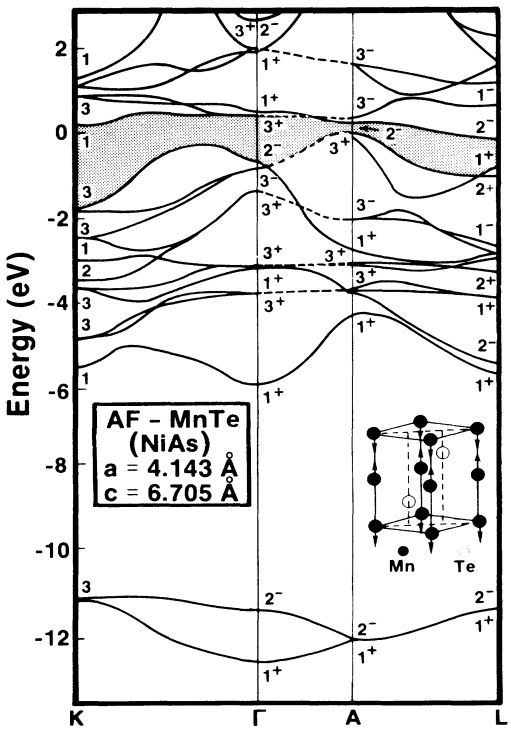

FIG. 16. Electronic band structure of AF MnTe in the NiAs structure. The zero of the energy is at the VBM (A_3^+ states). Dashed lines indicate doubly degenerate states. The band-gap region is shaded.

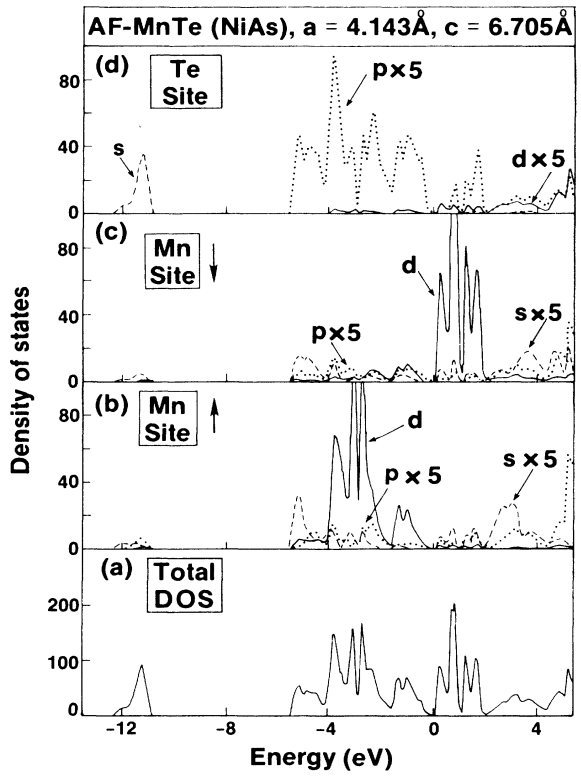

FIG. 17. Total DOS (a) and angular momentum and site projected local DOS (b)–(d) of AF MnTe in the NiAs structure.

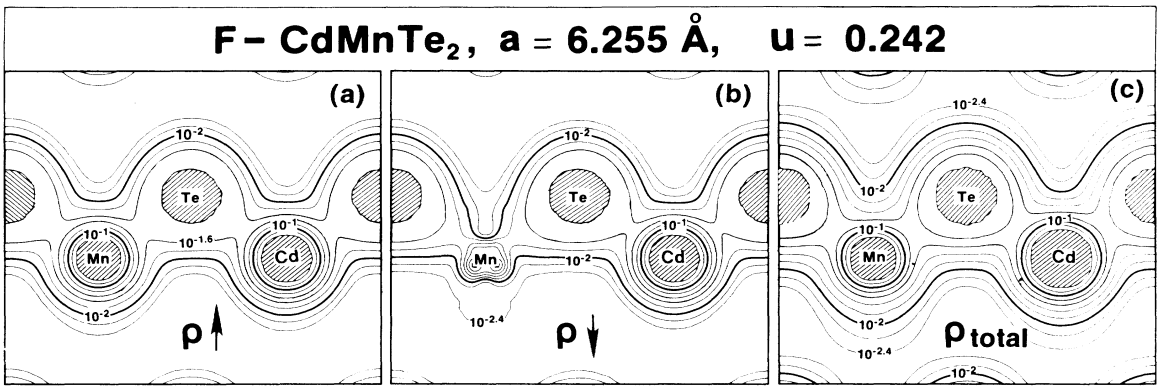

FIG. 18. Calculated charge density [in $e/(\text{a.u.})^3$] contours for F $CdMnTe_2$ on a plane defined by R(Mn—Te) and R(Cd—Te). [$(0,-1,1)$ if $u=0.25$]; (a) spin up, (b) spin down, and (c) total. A logarithmic scale is used, with a step size of $10^{0.2}$. Shaded regions highlight the covalent bonding.

the following discussion), the occupied Mn d states centered at a Mn atom have the symmetry $3^+,3^+,1^+$, but the empty states centered at the second Mn atom have the symmetry $2^-,3^-,3^-$, and the Te p states at the top of valence band have the symmetry $3^+,3^-$. p-d repulsion then raises the p states with 3^+ symmetry and lowers the p states with 3^- symmetry. This explains why the VBM in H-MnTe occurs at A point and why the direct band gap of MnTe is smaller than that of MnTe in ZB structures. Furthermore, because of the different symmetry, the electronic transition is more bandlike. This symmetry argument is also supported by the density of state plots for AF-ZB-MnTe [Figs. 14(a)—14(d)] and AF-H-MnTe [Figs. 17(a)—17(d)]. Figures 17(a) and 17(c) show for H-MnTe a bandlike DOS near the VBM with little d character, whereas Figs. 14(a) and 14(c) show for ZB MnTe a large DOS near the VBM with a pronounced d character. The bandwidth of the localized unoccupied Mn d band in the ZB structure (1.6 eV) is also smaller than that in the NiAs structure (3.0 eV), suggesting stronger multiplet effects in the former. In addition, because of the smaller band gap of AF-H-MnTe (1.3 eV), any intra-atomic transition ($\sim$2.2 eV) will be obscured by the fundamental transitions.

IX. CHARGE DISTRIBUTION

Figures 18 and 19 depict the calculated density contours of F $CdMnTe_2$ and AF-H-MnTe, respectively. In both cases, we find the partial ionic and partial covalent bonds connecting Mn—Te and Cd—Te atoms, typical to most II-VI semiconductors. From Figs. 18(a) and 18(b) and Fig. 19(a), which show the spin-up and spin-down charge densities, we see that the Mn $3d$ electron partici-

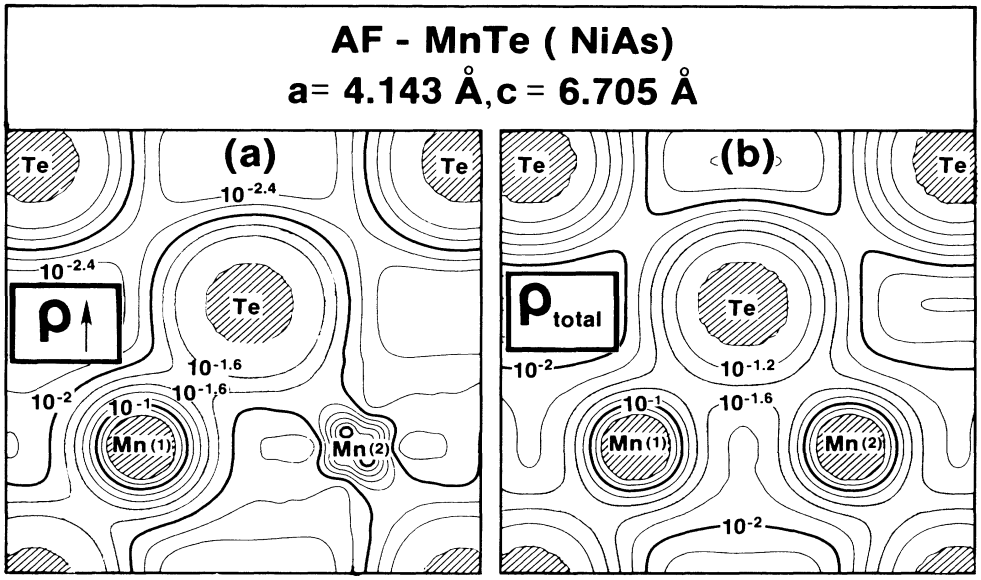

FIG. 19. Calculated charge density [in $e/(\text{a.u.})^3$] contours for AF MnTe in NiAs structure on the (110) plane; (a) spin up, (b) total. A logarithmic scale is used with a step size of $10^{0.2}$. Shaded regions highlight the covalent bonding.

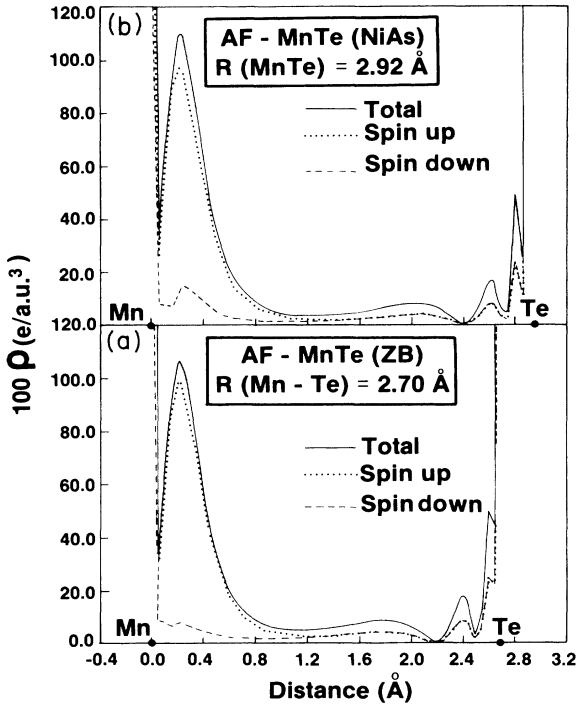

FIG. 20. Spin up (dotted lines), spin down (dashed lines) and total charge density (solid lines) plots along the Mn—Te bond for AF-ZB-MnTe (a); and AF MnTe in the NiAs structure (b).

pate strongly in bonding. Figures 20(a) and 20(b) show the charge density plot along the Mn—Te bond for AF-ZB-MnTe and for AF-H-MnTe, respectively. We find that the charge distribution along the Mn—Te bond is very similar in these two structures. The Mn d electrons are localized on the Mn atom and produce most of the spin density. The spin density vanishes beyond a distance of $R=1.3$ Å (which justifies the muffin-tin radii used in our calculation: $R_{\mathrm{MT}}=1.339$ Å for a ZB structure and $R_{\mathrm{MT}}=1.482$ Å for NiAs structure). Because of the larger distance of R(Mn—Te) in the NiAs structure, the covalent bonds in the hexagonal structure are slightly weaker than in the ZB structure.

X. MAGNETIC PROPERTIES

Because of the unfilled Mn $3d$ shell, permanent local magnetic moments are produced in semimagnetic semiconductors. Many of the interesting properties of semimagnetic semiconductors arise from the exchange interactions between the magnetic ions and the electrons (or holes) near the band edges.[4,5] In our calculation, the p-d hybridization is found to reduce the local magnetic moment of Mn from its free space value of $5.0\mu_B$ to about $4.30\mu_B$, and it even produces a small local magnetic moment of about $0.05\mu_B$ on the otherwise nonmagnetic Te and Cd sites in F $CdMnTe_2$. Because of the greater interaction of the Mn $3d_\uparrow$ and $3d_\downarrow$ orbitals in the AF phase, the Mn local magnetic moment is smaller than in the F phase. The calculated local magnetic moments within the MT spheres for F-ZB-MnTe, AF-ZB-MnTe, F $CdMnTe_2$, and AF-H-MnTe are given in Table VII. In the ferromagnetic phase the magnetic moment within each unit cell equals almost exactly $5\mu_B$. Comparing with the measured[80] magnetic moment of AF-H-MnTe, we find that the local-spin-density-functional theory (LSD) systematically underestimates the magnetic moment by about $0.6\mu_B$. This is consistent with underestimates of the localization of the Mn $3d$ electrons.

The tendency of $Cd_{1-x}Mn_xTe$ to form either a spin-glass-phase or an AF-phase alloy has been attributed to the Te mediated covalant spin interactions between Mn atoms through a superexchange mechanism.[16] The nearest-neighbor (NN) exchange interaction energy J_{NN} in the Heisenberg Hamiltonian[16] can be estimated from our total-energy calculation, assuming that J_{NN} is independent of concentration[16] and that the next-nearest-neighbor (NNN) interaction J_{NNN} is much smaller, compared with[14] J_{NN}. From the Heisenberg model, the energy change per magnetic atom due to the spin flip of the magnetic atom is

$$\Delta E = 2MJ_{\mathrm{NN}}S(S+1)\ , \tag{10}$$

where M is the number of nearest neighbors that changed spin direction and S is the spin quantum number. For the first type AF spin ordering in the fcc lattice, we have $M=8$. Using the calculated total-energy difference between F and AF MnTe (-0.19 eV/pair; Fig. 3 and Table I), and taking a local magnetic moment of $\mu=5\mu_B$, we find $J_{\mathrm{NN}}=-16$ K. This value compares satisfactorily with the experimental neutron diffraction value[15] of -7.5 K and with previous calculations, giving -12 K (using perturbation theory[16]) and -17 K (from a total-energy calculation[16]). Even though the agreement is good, considering the uncertainties in the relative energies of F and AF MnTe and in the magnetic moment, we find that an uncertainty for J_{NN} could be as large as about 8 K.

It has been shown[17] that ferromagnetic band-structure calculation of $Cd_{1-x}Mn_xTe$ can also be used to estimate the exchange constants $N_0\alpha$ and $N_0\beta$. Assuming the usual Kondo interactions, $N_0\alpha$ and $N_0\beta$ are defined[5] as

$$N_0\alpha=\frac{\Delta E_c}{x\langle S_z\rangle};\quad N_0\beta=\frac{\Delta E_v}{x\langle S_z\rangle}\ , \tag{11}$$

where ΔE_v and ΔE_c are the band-edge spin splittings of the valence bands and conduction bands (s states), respec-

TABLE VII. Calculated local magnetic moments (in Bohr magneton μ_B). $R_{\mathrm{MT}}=1.48$ Å for the NiAs structure, $R_{\mathrm{MT}}=1.34$ Å for the cubic phases.

Site	AF MnTe(NiAs)	F $CdMnTe_2$	F-ZB-MnTe	AF-ZB-MnTe
Mn	4.17	4.30	4.39	4.10
Te	0	0.08	0.14	0
Cd		0.04		

TABLE VIII. Calculated exchange interaction coefficients in comparison with experimental data (see also the text).

System	J_{NN} (K)	$N_0\alpha$ (eV)	$N_0\beta$ (eV)
MnTe (ZB)	−16	0.48	−1.16
$CdMnTe_2$ (CuAu-I)		0.54	−1.30
ASW[a]	−17	0.33	−1.05
Experiment	−7.5[b]	0.22[c]	−0.88[c]

[a]Reference 17.
[b]Reference 15.
[c]Reference 5.

tively, and $\langle S_z \rangle$ is the average Mn spin. Using the calculated band structure and $\langle S_z \rangle$ value for F MnTe and F $CdMnTe_2$, we have calculated $N_0\alpha$ and $N_0\beta$. Results are listed in Table VIII and compared with experimental data and previous calculations by Hass *et al.*[17] The agreement is satisfactory. We find that the exchange constants increase with decreasing Mn composition because of the enhancement in the symmetry induced interaction between band-edge states and Mn d states; this trend agrees with the experimental data.[5]

The overestimation of the exchange interaction energy constants is a characteristic of the LSD calculation.[81] Since LSD underestimates the exchange splitting of Mn $3d_\uparrow$ and $3d_\downarrow$ states, it also reduces the p-d energy separation (see Fig. 7). This will increase p-d hybridization; consequently, the superexchange coupling between Mn ions and electrons increases.

XI. CONCLUSION

We have performed total-energy and band-structure calculations for the prototypical semimagnetic semiconductor $Cd_{1-x}Mn_xTe$. We find that the alloy environment stabilized a hitherto unknown ZB phase on MnTe and that the electronic structure of $Cd_{1-x}Mn_xTe$ is related to this ZB phase of MnTe, but not to the hexagonal phase. We find that the ZB phase of MnTe is metastable compared with its NiAs phase and predict that the ordered $CdMnTe_2$ can exist only in the ferromagnetic form. We find that in this ferromagnetic form the system has a negative p-d exchange splitting and small magnetic moment even on the nonmagnetic ions (Cd,Te). The occupied Mn $3d$ states are predicted to be partially localized, located at $E_v-2.5$ eV, and strongly hybridized with Te $5p$ states. The difference in the nature of the electronic transitions in hexagonal MnTe and $Cd_{1-x}Mn_xTe$ is explained in terms of their different underlying symmetry properties. Exchange interaction coefficients have been estimated from our first-principles calculation. We see that a better exchange correlation potential is required to calculate these constants accurately.

ACKNOWLEDGMENT

This work was supported by the Office of Energy Research, Materials Science Division, U.S. Department of Energy, under Grant No. DE-AC02-77-CH00178.

APPENDIX

Considerable confusion exists in the literature regarding the chemical trends in the cohesive energies and bond strengths of column-II chalcogenides and halides. Using various calorimetric and spectroscopic results, we show here the trends in the data.

We define the cohesive (c) energy of a compound MX with respect to the *isolated and neutral atoms* M and X as

$$-E_c(MX)=E_s(MX)-E_a(M)-E_a(X)\ , \tag{A1}$$

where $E_s(MX)$ denotes the total energy of the solid(s) MX at zero pressure and temperature, and E_a is the atomic (a) ground-state energies. $E_c(MX)$ can be evaluated from the measured enthalpy of formation $\Delta H(MX)$,

$$\Delta H(MX)=H_s(MX)-H_e(M)-H_e(X)\ , \tag{A2}$$

TABLE IX. Observed formation enthalpies $\Delta H(MX)$, elemental cohesive energies E_c, and the compound cohesive energy $E_c(MX)$ for group-II and Mn chalcogenides.

System MX	$-\Delta H$ at 300 K (Kcal/mol)[a]	$E_c(M)$ (Kcal/mol)[a]	$E_c(X)$ (Kcal/mol)[a]	$E_c(MX)$ (eV/pair)
MgS	84.0	34.7	65.8	8.00
MgSe	65.2	34.7	51.8	6.58
MgTe	50.0	34.7	51.4	5.90
ZnS	49.1	31.1	65.8	6.33
ZnSe	38.0	31.1	51.8	5.25
ZnTe	28.5	31.1	51.4	4.81
CdS	35.7	26.7	65.8	5.56
CdSe	34.6	26.7	51.8	4.91
CdTe	24.3	26.7	51.4	4.44
MnS	51.0	67.4	65.8	7.99
MnSe	37.0	67.4	51.8	6.78
MnTe	26.6	67.4	51.4	6.31

[a]Reference 61.

TABLE X. Observed formation enthalpies $\Delta(MX_2)$, elemental cohesive energies E_c, the ionic correction $\Delta(M,X)=I_M^{(1)}+I_M^{(2)}-2\chi_X$, and the compound cohesive energy $E_c(MX_2)$ and its "lattice energy" [see Eq. (A4)].

System MX_2	$-\Delta H(MX_2)$ at 300 K (Kcal/mol)[a]	$E_c(M)$ (Kcal/mol)[a]	$2E_c(X)$ (Kcal/mol)[a]	$E_c(MX_2)$ (eV/mol)	$-U(MX_2)$ (eV/mol)	$\Delta(M,X)$ (eV/mol)[b]
CaF_2	292	42.5	38.7	16.17	27.34	11.17
$CaCl_2$	190	42.5	64.4	12.89	23.64	10.75
$CaBr_2$	163	42.5	56.4	11.37	22.62	11.25
CaI_2	128	42.5	51.2	9.60	21.46	11.86
MnF_2	(192)	67.4	38.7	12.93	29.21	16.28
$MnCl_2$	115	67.4	64.4	10.71	26.56	15.85
$MnBr_2$	92	67.4	56.4	9.36	25.71	16.35
MnI_2	58	67.4	51.2	7.66	24.62	16.96
ZnF_2	182	31.1	38.7	10.92	31.48	20.56
$ZnCl_2$	99	31.1	64.4	8.44	28.58	20.14
$ZnBr_2$	79	31.1	56.4	7.21	27.85	20.64
ZnI_2	50	31.1	51.2	5.73	26.96	21.23

[a]Reference 61.
[b]References 61 and 84.

[where H_e are enthalpies of the elements (e) in their condensed phase], and from the elemental cohesive energies $E_c(M)$ and $E_c(X)$, as

$$E_c(MX)=-\Delta H(MX)+E_c(M)+E_c(X)\ . \tag{A3}$$

Table IX depicts the measured $\Delta H(MX)$ values (taken from the compilation of Kubachevski and Alcock[63]), the observed cohesive energies $E_c(M)$ and $E_c(X)$ of Brewer (compiled by Kittle[63]), and the calculated values $E_c(MX)$ from Eq. (A3). We see that for a fixed anion, the cohesive energy *decreases* in the series $MgX\rightarrow ZnX\rightarrow CdX$ of divalent cations, whereas the cohesive energy of the Mn compounds is *larger* than those of the corresponding group-II cations (except MgS). This trend is explained in Sec. IV in terms of a competition of spin polarization effects (favoring a stronger cohesion in $M^{II}X$) and d-electron bonding effects (favoring a stronger cohesion of MnX compounds). Our calculation indeed predicts that $E_c(\mathrm{MnTe})-E_c(\mathrm{CdTe})=2.7$ eV, compared with the observed value of approximately 1.9 eV at room temperature.

Numerous textbooks (e.g., see Ref. 82, Fig. 9.16, or Ref. 83, Fig. 55) depict instead of $E_c(MX)$ of Eq. (A1) the *lattice energies* $U(MX)$ that are related to cohesive energies with respect to *free ions*. For example, for the dihalides MX_2 (X=F,Cl,Br,I), one has the relationship

$$-U(MX)=E_c(MX)+I_M^{(1)}+I_M^{(2)}-2\chi_X\ , \tag{A4}$$

where $I_M^{(i)}$ is the ith ionization energy for the metal and χ_X is the (first) electron affinity of the nonmetal. The strong variations in $\Delta(M,X)=[I_M^{(1)}+I_M^{(2)}-2\chi_X]$ along a MX series then obscure the trends of $E_c(MX)$. For instance, for the fluorides MX_2 one has $\Delta(\mathrm{Ca,F})=11.2$ eV, $\Delta(\mathrm{Mg,V})=15.9$ eV, $\Delta(\mathrm{Zn,F})=20.6$ eV, $\Delta(\mathrm{Cd,F})=19.1$ eV, and $\Delta(\mathrm{Mn,F})=16.3$ eV (using ionization potentials and electron affinities from Refs. 84 and 61). Hence, whereas the lattice energies $U(MX)$ suggest that CaX_2 is "less stable" than MnX_2, which in turn is "less stable" than ZnX_2 (Ref. 82, Fig. 9.16), the actual cohesive energies have the reverse trend. This is depicted in Table X.

[1]R. R. Galazka, *Physics of Semiconductors—1978 (Edinburgh), Proceedings of the 14th International Conference on the Physics of Semiconductors,* Inst. Phys. Conf. Ser. No. **43**, edited by B. L. H. Wilson (Institute of Physics and Physical Society, London, 1979), p. 133.
[2]J. K. Furdyna, J. Appl. Phys. **53**, 7637 (1982).
[3]R. R. Galazka, S. Nagata, and P. H. Keesom, Phys. Rev. B **22**, 3344 (1980).
[4]J. A. Gaj, J. Ginter, and R. R. Galazka, Phys. Status Solidi B **89**, 655 (1978); J. A. Gaj, R. R. Galazka, and N. Nawrocki, Solid State Commun. **25**, 193 (1978); A. Mycielski and J. Mycielski, J. Phys. Soc. Jpn. **49**, Suppl. A, 807 (1980); A. Golnik, J. A. Gaj, M. Nawrocki, R. Planel, and C. Benoita à la Guillaume, J. Phys. Soc. Jpn. **49**, Suppl. A, 819 (1980).
[5]J. A. Gaj, R. Planel, and G. Fishman, Solid State Commun. **29**, 435 (1979).
[6]N. T. Khoi and J. A. Gaj, Phys. Status Solidi B **83**, K133 (1977).
[7]Y. R. Lee and A. K. Ramdas, Solid State Commun. **51**, 861 (1984).
[8]M. Zimnal-Starnawska, M. Podgorny, A. Kisiel, W. Giriat, M. Demianiuk, and J. Zmija, J. Phys. C **17**, 615 (1984).
[9]J. E. Morales Toro, W. M. Beck, B. I. Wang, U. Debska, and J. W. Richardson, Solid State Commun. **52**, 41 (1981).

[10]P. Oelhafen, M. P. Vecchi, J. L. Freeouf, and V. L. Moruzzi, Solid State Commun. **44**, 1547 (1982).

[11]*Numerical Data and Functional Relationships in Science and Technology,* Vol. 17a of *Landolt-Börnstein,* edited by O. Madelung, M. Schulz, and H. Wiess (Springer-Verlag, Berlin, 1982), pp. 333—348; *Numerical Data and Functional Relationships in Science and Technology,* Vol. 17b of *Landolt-Börnstein,* edited by O. Madelung (Springer-Verlag, Berlin, 1982), pp. 244—252.

[12]A. Zunger, Annu. Rev. Mater. Sci. **15**, 411 (1985); and in *Solid State Physics,* edited by H. Ehrenreich and D. Turnbull (Academic, New York, in press); V. A. Singh and A. Zunger, Phys. Rev. B **31**, 3729 (1985).

[13]A. Pajaczkowska, Prog. Cryst. Growth Charact. **1**, 289 (1978).

[14]M. Escorne, A. Manger, R. Triboulet, and J. L. Tholense, Physica **107B**, 309 (1981).

[15]T. M. Giebultowicz, J. J. Rhyne, W. Y. Ching, and D. L. Huber, J. Appl. Phys. **57**, 3415 (1985).

[16]B. E. Larson, K. C. Hass, M. Ehrenreich, and A. E. Carlsson, Solid State Commun. **56**, 347 (1985).

[17]K. C. Hass, B. E. Larson, H. Ehrenreich, and A. E. Carlsson, J. Magn. Magn. Mater. **54-57**, 1283 (1986).

[18]A. K. Bhattacharjee, G. Fishman, and B. Cogblin, Physica **117&118B**, 449 (1983).

[19]C. Webb, M. Kaminska, M. Lichtensteiger, and J. Lagowski, Solid State Commun. **40**, 609 (1981).

[20]B. A. Orlowski, Phys. Stat. Solidi B **95**, K31 (1979).

[21]M. P. Vecchi, W. Giriat, and L. Videla, Appl. Phys. Lett. **38**, 99 (1981).

[22]J. P. Laseary, J. Diouri, M. El Amran, and D. Coquillat, Solid State Commun. **47**, 709 (1983).

[23]E. Müller, W. Gebhart, and W. Rehwald, J. Phys. C **16**, L1141 (1983).

[24]R. A. Abren, W. Giriat, and M. P. Vecchi, Phys. Lett. **85**, 399 (1981).

[25]E. I. Grancharova, J. P. Lascaray, J. Diouri, and J. Allegre, Phys. Status Solidi B **113**, 503 (1982); P. Lemasson, B. L. Wu, R. Triboulet, and J. Gautron, Solid State Commun. **47**, 669 (1983).

[26]J. W. Allen, G. Lucovsky, and J. C. Mikkesen, Jr., Solid State Commun. **24**, 367 (1983).

[27]M. T. Czyzyk and M. Podgorny, Proc. Conf. Phys. **6**, 448 (1983).

[28]M. Podgorny and J. Oeskiewicz, J. Phys. C **16**, 2547 (1983), and reference therein.

[29]L. M. Sandratskii, R. F. Egorov, and A. A. Berdyshev, Phys. Status Solidi B **140**, 103 (1981).

[30]R. A. de Groot, Ph.D. thesis, University of Groeningen, 1976 (unpublished).

[31]S.-H. Wei and A. Zunger, Phys. Rev. Lett. **56**, 2391 (1986).

[32]P. Hohenberg and W. Kohn, Phys. Rev. **136**, B864 (1964); W. Kohn and L. J. Sham, Phys. Rev. **140**, A1133 (1965).

[33]L. Hedin and B. I. Lundqvist, J. Phys. C **4**, 2064 (1971); V. von Barth and L. Hedin, *ibid.* **5**, 1629 (1972).

[34]B. Ray, *II-VI Compounds* (Pergamon, Oxford, 1969).

[35]N. K. Abrikosov, V. F. Bankine, L. V. Poretskaya, L. E. Shelimova, and E. V. Skudnova, *Semiconducting II-VI, IV-VI, and III-V Compounds* (Plenum, New York, 1969).

[36]A. G. Fischer and R. J. Paff, J. Phys. Chem. Solids **23**, 1479 (1962).

[37]N. A. Goryunova, V. A. Kotovich, and V. A. Frank-Kamenetskii, Zh. Tekh. Fiz. **25**, 2491 (1955); S. Forque, R. Goodrich, and A. Cope, RCA Rev. **12**, 335 (1951).

[38]R. Hill and A. N. Casperd (unpublished); M. V. Kurik and N. I. Vitrikhovskii, Phys. Status Solidi **16**, K139 (1966); D. Bonnet, *ibid.* **3a**, 913 (1970); K. Ohata, J. Saraie, and T. Tanaka, Jpn. J. Appl. Phys. **12**, 1198 (1973); N. I. Vitrikhovskii and I. B. Mizetskaya, Fiz. Tverd. Tela (Leningrad) **1**, 996 (1959) [Sov. Phys.—Solid State **1**, 912 (1959)].

[39]M. S. Brodin, N. I. Vitrikhouskii, A. A. Kipen, and I. B. Mizetskaya, Fiz. Tek. Poluprov. **6**, 698 (1972) [Sov. Phys.—Semicond. **6**, 601 (1972)]; H. Tai, S. Nakashima, and S. Hori, Phys. Status Solidi **30a**, K115 (1975); G. Hodes, J. Menassen, and D. Cahen, J. Am. Chem. Soc. **102**, 5964 (1980); A. J. Strauss and J. Steininger, J. Electrochem. Soc. **117**, 1420 (1970); A. D. Stukes and G. Farrell, J. Phys. Chem. Solids **25**, 477 (1964).

[40]M. Hansen and K. Anderko, *Constitution of Binary Alloys,* 2nd ed. (McGraw-Hill, New York, 1968).

[41]A. J. Majumdar, Am. Mineralogist **50**, 1121 (1965).

[42]A. Kremhller, A. K. Livine, and G. Gashurov, J. Electrochem. Soc. **107**, 1 (1960).

[43]M. V. Kot and V. A. Mshenskii, Izv. Akad. Nauk. SSSR, Ser. Fiz. **28**, 1067 (1964); D. A. Nelson, C. J. Summers, and C. R. Whitsett, J. Electron, Mater. **6**, 507 (1977); C. J. Summers and J. G. Broerman, Phys. Rev. B **21**, 559 (1980); A. Kalb and V. Leute, Phys. Status Solidi **5a**, K199 (1971); M. E. Cruceanu and D. Niculescu, C. R. Acad. Sci. (France) **261**, 935 (1965).

[44]H. Schnaase, Z. Phys. Chem. **20B**, 89 (1933); H. Wiedemeier and A. Khan, Trans. Metall. Soc. AIME **242**, 1969 (1968).

[45]W. C. Cook, J. Am. Ceram. Soc. **51**, 518 (1968).

[46]R. Juza, A. Rabenau, and G. Pascher, Z. Anorg. Allg. Chem. **285**, 61 (1956).

[47]R. T. Delves and B. Levis, J. Phys. Chem. Solids **24**, 549 (1963); A. H. J. Sadeek, Ph.D. thesis, Rensselaer Institute, 1971 (unpublished).

[48]W. D. Johnston and A. E. Sestrich, J. Inorg. Nucl. Chem. **19**, 229 (1961); V. G. Vanyarkho, V. P. Zlomanov, and A. V. Novoselova, Izv. Akad. Nauk. SSSR, Neorg. Mater. **6**, 1257,1534 (1970) [Inorg. Mater. **6**, 1102, 1352 (1970)], postulated a wurtzite and sphalerite phases of MnTe but there is no evidence for them in the phase diagram of Johnston and Sestrich.

[49]D. J. Chadi, J. P. Walter, M. L. Cohen, Y. Petroff, and M. Balkanski, Phys. Rev. B **5**, 3058 (1972).

[50]L. Tomassen, D. R. Mason, G. D. Rose, J. C. Sarace, and G. A. Schmitt, J. Electrochem. Soc. **110**, 1127 (1963).

[51]A. Balzarotti, M. Czyzyk, A. Kisiel, N. Motta, M. Podgorny, and M. Zimnal-Starnawska, Phys. Rev. B **30**, 2295 (1984).

[52]J. C. Woolley, in *Compound Semiconductors,* edited by R. K. Willardson and H. L. Goering (Reinhold, New York, 1962), p. 3.

[53]G. P. Srivastava, J. L. Martins, and A. Zunger, Phys. Rev. B **31**, 2561 (1985).

[54]J. E. Jaffe and A. Zunger, Phys. Rev. B **29**, 1882 (1984).

[55]S.-H. Wei, H. Krakauer, and M. Weinert, Phys. Rev. B **32**, 7792 (1985), and references therein.

[56]C. Umrigar and J. Wilkins, Phys. Rev. Lett. **54**, 1551 (1985).

[57]D. J. Chadi and M. L. Cohen, Phys. Rev. B **8**, 5747 (1973).

[58]The 12 **k** points are uniformly distributed in the irreducible sector of the first BZ, they are $(-\frac{1}{2},\frac{1}{2},\pm\frac{3}{8})$, $(-\frac{1}{2},\frac{1}{2},\pm\frac{1}{8})$, $(-\frac{1}{4},0,\pm\frac{3}{8})$, $(-\frac{1}{4},0,\pm\frac{1}{8})$, $(\frac{1}{2},-\frac{1}{4},\frac{3}{8})$, $(\frac{1}{2},-\frac{1}{4},-\frac{1}{8})$, $(0,0,\frac{3}{8})$, $(0,0,-\frac{1}{8})$ in the reciprocal lattice units.

[59]O. Jepsen and O. K. Andersen, Solid State Commun. **9**, 1763 (1971); G. Lehman and M. Taut, Phys. Status Solidi **54**, 469 (1972).

[60]Here we have assumed that $\eta=c/a=1$, since in the alloy en-

vironment there is no special direction (i.e., no c direction). This parameter η along with u can be used to minimize strain energy in ordered alloys arising from bond-length and bond-angle mismatch. See also, G. P. Srivastava, J. L. Martins, and A. Zunger, Phys. Rev. B **31**, 2561 (1985).

[61]W. A. Harrison, *Electronic Structure and Properties of Solids* (Freeman, San Francisco, 1980), p. 174.

[62]A. Fazzio, M. J. Caldas, and A. Zunger, Phys. Rev. B **30**, 3430 (1984); H. Katayama-Yoshida and A. Zunger, *ibid.* **32**, 8317 (1985).

[63]O. Kubachevski and C. B. Alcock, *Metallurgical Thermochemistry,* 5th ed. (Pergamon, New York, 1979), pp. 267—322; C. Kittel, *Solid State Physics,* 5th ed. (Wiley, New York, 1976), pp. 74 and 89.

[64]We have assumed energy difference between AF $CdMnTe_2$ and F $CdMnTe_2$ is half of the difference between AF MnTe and F MnTe. The actual number may even be smaller [N.E. Christensen (private communication)].

[65]At low Mn concentration ($x < 0.1$), however, Mn is inferred to have an ideal random distribution. See R. L. Aggarwal, S. N. Jasperson, P. Becla, and R. R. Galazka, Phys. Rev. B **32**, 5132 (1985); Y. Shapira, S. Foner, D. H. Ridgley, K. Dwight, and A. Wold, *ibid.* **30**, 4021 (1984).

[66]L. Martins and A. Zunger, Phys. Rev. Lett. **56**, 1400 (1986).

[67]V. L. Morozzi, J. F. Janak, and A. R. Williams, *Calculated Electronic Properties of Metals* (Pergamon, New York, 1978).

[68]M. Taniguchi, L. Ley, R. L. Johnson, J. Ghijsen, and M. Cardona, Phys. Rev. B **33**, 1206 (1986); L. Ley, M. Taniguchi, J. Ghijsen, R. L. Johnson, and A. Fujimori (unpublished).

[69]N. A. Cade and P. M. Lee, Solid State Commun. **56**, 637 (1985).

[70]L. Ley, R. A. Pollak, F. R. McFeely, S. P. Kowalczyk, and D. A. Shirley, Phys. Rev. B **9**, 600 (1974); N. J. Shevchik, J. Tejeda, and M. Cardona, *ibid.* **9**, 2627 (1974).

[71]A. Zunger, Phys. Rev. Lett. **50**, 1215 (1983); M. Caldas, A. Fazzio, and A. Zunger, Appl. Phys. Lett. **45**, 671 (1984).

[72]These are averaged values for spin-up and spin-down states.

[73]A. Zunger and A. J. Freeman, Phys. Rev. B **16**, 2901 (1977).

[74]J. C. Slater, *The Self-Consistent Field for Molecules and Solids* (McGraw-Hill, New York, 1974).

[75]J. P. Perdew and A. Zunger, Phys. Rev. B **23**, 5048 (1981).

[76]A. Zunger and U. Lindefelt, Solid State Commun. **45**, 343 (1983).

[77]Y. R. Lee, A. K. Ramdas, and R. L. Aggarwal, Phys. Rev. B **33**, 7383 (1986).

[78]J. Calas, J. P. Lascaray, M. Averous, F. El Darazi, and D. Coluillat, Solid State. Commun. **54**, 371 (1985).

[79]L. F. Mattheiss, Phys. Rev. B **10**, 995 (1974).

[80]N. Kunitomi, Y. Hamaguchi, and S. Anzai, J. Phys. (Paris) **25**, 568 (1964).

[81]T. Oguchi, K. Terakura, and A. R. Williams, J. Appl. Phys. **55**, 2318 (1984).

[82]J. E. Huheey, *Inorganic Chemistry,* 3rd ed. (Harper and Row, New York, 1983), p. 387.

[83]B. N. Figgis, *Introduction to Ligand Fields* (Interscience, New York, 1966), p. 83.

[84]L. H. Ahrens, *Ionization Potentials* (Pergamon, New York, 1983), p. 97.